INFORMATION TO USERS

This dissertation was produced from a microfilm copy of the original document. While the most advanced technological means to photograph and reproduce this document have been used, the quality is heavily dependent upon the quality of the original submitted.

The following explanation of techniques is provided to help you understand markings or patterns which may appear on this reproduction.

1. The sign or "target" for pages apparently lacking from the document photographed is "Missing Page(s)". If it was possible to obtain the missing page(s) or section, they are spliced into the film along with adjacent pages. This may have necessitated cutting thru an image and duplicating adjacent pages to insure you complete continuity.

2. When an image on the film is obliterated with a large round black mark, it is an indication that the photographer suspected that the copy may have moved during exposure and thus cause a blurred image. You will find a good image of the page in the adjacent frame.

3. When a map, drawing or chart, etc., was part of the material being photographed the photographer followed a definite method in "sectioning" the material. It is customary to begin photoing at the upper left hand corner of a large sheet and to continue photoing from left to right in equal sections with a small overlap. If necessary, sectioning is continued again — beginning below the first row and continuing on until complete.

4. The majority of users indicate that the textual content is of greatest value, however, a somewhat higher quality reproduction could be made from "photographs" if essential to the understanding of the dissertation. Silver prints of "photographs" may be ordered at additional charge by writing the Order Department, giving the catalog number, title, author and specific pages you wish reproduced.

University Microfilms

300 North Zeeb Road
Ann Arbor, Michigan 48106

A Xerox Education Company

The effect of applied electric fields on diffusion controlled scaling kinetics

by

Jay William Hinze

A Dissertation Submitted to the
Graduate Faculty in Partial Fulfillment of
The Requirements for the Degree of
DOCTOR OF PHILOSOPHY

Major: Metallurgy

Approved:

Signature was redacted for privacy.

In Charge of Major Work

Signature was redacted for privacy.

For the Major Department

Signature was redacted for privacy.

For the Graduate College

Iowa State University
Ames, Iowa

1973

TABLE OF CONTENTS

SELECTED LIST OF SYMBOLS

A	cross-sectional area
E_{TH}	thermodynamic emf
E_W	open circuit emf
F	Faraday's constant
I_j	steady state electrical current conducted by the jth species where j = 1, 2, 3 corresponding to cations, anions and electrons, respectively
I_T	steady state total current
J_{X_2}	flux of the neutral oxidant species
k	Wagner's scaling rate constant
k_n	scaling rate constant due to neutral oxidant species
L	scaling layer thickness
$\dot{L}$	rate of scale thickening or thinning
N	Avagadro's number
$\dot{n}$	rate of scale formation or decomposition
P_{X_2}	partial pressure of X_2 gas. " refers to high pressure side of the cell; ' refers to the low pressure side
$P_{\oplus}$	P_{X_2} at which the ionic and hole conductivities are equal
r	the ratio $[I_1 + I_2]/I_3$
R	gas constant
T	temperature ^oK
t	time
t_j	transference number of the jth species
t_{ion}	ionic transference number

$\bar{t}_{ion}$ spatial average of the ionic transference number

$\bar{v}$ equivalent volume

V_{Halt} voltage necessary to arrest scale thickening or thinning

V_T cell voltage

z_j valence of the jth species

η_j electrochemical potential of the jth species

μ_{X_2} chemical potential of the nonmetal species. " refers to high chemical potential side of cell; ' refers to low chemical potential side

μ_M chemical potential of the metal

σ_j electrical conductivity of the jth species

σ_j^o electrical conductivity of the jth species at P_{X_2} = 1 atm

σ_{ion} ionic conductivity

σ_T total conductivity

σ_T^o total conductivity at P_{X_2} = 1 atm

$\bar{\sigma}_T$ spatial average of the total conductivity

INTRODUCTION

The effect of applied electric fields on the oxidation of metals has received a considerable amount of attention in the literature in recent years. The original study in this area was conducted in 1955 by Uhlig and Brenner (1) on copper oxidation where electric fields were applied across the oxidizing copper specimens with the use of the condenser arrangement shown in Figure 1a. Uhlig and Brenner, however, were unable to influence the oxidation rate of copper by applying electric fields as high as 15 KV/cm. In a more recent paper Cismaru and Cismaru (2) were unable to influence the oxidation rate of zinc by applying fields across cells of the type shown in Figure 1b. It was later suggested by Jorgensen (3) that one would not expect to influence the oxidation rate using the cell arrangements of Uhlig and Brenner (1) and Cismaru and Cismaru (2). This is because the entire voltage drop would occur across the insulating air gap between the condenser plates and not across the oxide scale. Jorgensen proposed instead that the electrodes should be contacted directly to the oxidizing metal and the outside surface of the oxide scale so that the entire voltage drop would occur across the scale.

In later papers concerning the effect of applied electric fields on metal oxidation, the fields were coupled directly to the oxide scales as shown schematically in Figure 1c. A number of investigators have used this arrangement to determine the mechanism of metal oxidation. For example, Jorgensen (3, 4) determined that the oxidation of silicon is diffusion controlled and that oxygen ions are the mobile

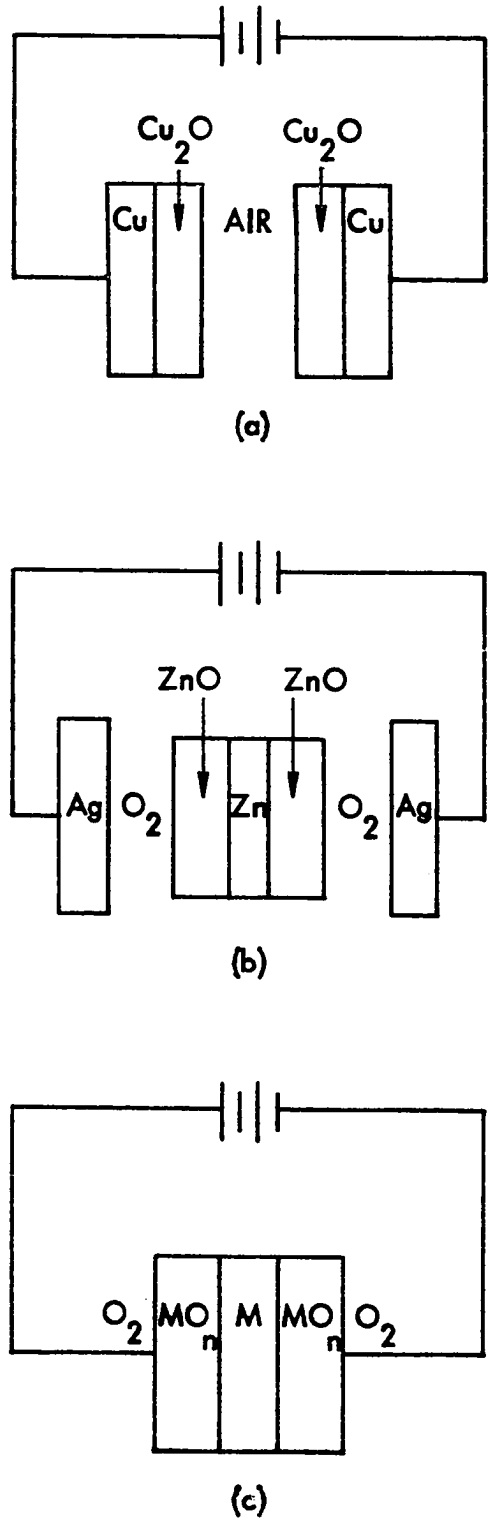

Figure 1. Experimental cell arrangement for applied electric field experiments. a) Uhlig and Brenner (1). b) Cismaru and Cismaru (2). b) Recent studies.

species. Laverty and Ryan (5) made further studies on silicon oxidation and deduced that oxygen in the form of ions and neutral molecules could be mobile. Jorgensen (6) studied the oxidation of zinc and found diffusion of zinc ions to be rate controlling. Bradhurst, Draley and Van Drunen (7) studied the oxidation of zirconium and found the reaction to be diffusion controlled with electrons being the rate controlling species. In a recent work Berkowitz et al. (8) studied the oxidation mechanism of nickel base alloys by applying electric fields across seeded plasma gases. Since such gases are electrically conductive, a cell arrangement similar to that of Uhlig and Brenner (1) was used effectively to influence the oxidation rate.

Externally applied electric fields have also been used in low temperature studies by Ritchie and co-workers to determine the mechanism of oxidation of zinc (9), tungsten (9), aluminum (10) and nickel (11). Krishnamoorthy and Sircar (12) used this technique to study the oxidation of copper. These latter studies were conducted at low temperatures for thin oxide films where diffusion through the scale was not rate controlling. Results were discussed in terms of the Mott-Cabrera theory of oxidation (13) and are not of much interest in the present work which is concerned with diffusion controlled scaling (oxidation) reactions.

Some of the interpretations offered for the foregoing works have involved rather pointed controversies. For example, Jorgensen's study on silicon oxidation (3) was criticized by Raleigh (14), who claimed that it is impossible to 1) influence the normal oxidation rate of metals by the application of external electric fields and 2) determine

the mechanism of normal oxidation with this technique. This criticism sparked a rather vigorous exchange of letters to the editor of the Journal of the Electrochemical Society (15, 16). A considerable amount of misunderstanding was evidenced which seems to have left the mechanism of silicon oxidation and mass transport in SiO_2 uncertain even up to the present time (17, 18).

The effect of applied electric fields on the oxidation of metals has been treated theoretically by several authors including Fromhold (19-21), Anderson and Ritchie (22), Kröger (23) and Wagner (24). Only the works of Kröger and Wagner apply for diffusion controlled scaling kinetics with the latter work being in the form of an unpublished memo. Jorgensen (25) has recently published a review article on the subject in which the features of Wagner's treatment (24) are summarized.

The treatments of Kröger (23) and Wagner (24) extend Wagner's theory of oxidation (26) under open circuit conditions to include the effect of applied electric fields on diffusion controlled scaling kinetics. Kröger (23) derived an equation describing the rate of scale growth at the differential equation level which may be written as

$$\dot{L} = \bar{v}\bar{t}_{ion} I_T/FA + k/L \qquad [1]$$

where $\dot{L}$ is the rate of scale formation in cm/sec, $\bar{v}$ is the equivalent volume, $\bar{t}_{ion}$ is the spatial average of the ionic transference number, I_T is the total current, F is Faraday's number, A is the cross sectional area of the scale, k is Wagner's rational scaling rate constant (26)

in cm^2/sec and L is the scale thickness*. Because the parameter $\bar{t}_{ion}$ is a spatial average (and not the usual average on chemical potential), it is generally time dependent. This makes it impossible to infer from Eq. [1] the scale thickness as a function of time unless of course additional simplifying assumptions are involved. Wagner (24) derived a general expression for the scale thickness in terms of ionic fluxes and external current which is not very useful for obtaining the time dependence of the scale thickness. Two limiting cases were treated in which the total current and the ionic fluxes vanish.

Thus, neither the analysis of Kröger nor that of Wagner yields formulas for scale thickness, cell voltage or total current as functions of time. This is unfortunate because such formulas would be very useful for analyzing experimental data. Plots of voltage and current as functions of time would be especially useful because one could avoid interruptions and other inconveniences involved in the measurement of scale thickness or weight changes with time. Furthermore, neither of the above analyses allow for the migration of neutral species. A certain amount of experimental evidence suggests that neutral migration is exhibited in PbO (27) and in SiO_2 (5, 14, 28-30). Because of the controversy involving the nature of mass transport in SiO_2, it would be helpful to develop theoretical formulas for electric field scaling kinetics which include the effects of neutral fluxes.

The purposes of the present research are as follows: 1) It is the main goal of the present work to develop a theory which quantitatively

---

*The symbols used in this work are defined on page v.

predicts the influence of applied electric fields on diffusion controlled scaling kinetics. Equations will be derived which predict scale thickness, cell voltage and total current as functions of time for various applied electric field conditions. 2) These theoretical equations will be used to predict the effect of applied electric fields on silicon oxidation and silver bromination for which the normal scaling reactions are believed to be diffusion controlled (3, 4, 14, 31). 3) Experiments will be conducted on silicon oxidation and silver bromination in order to determine the applicability of the theoretical analysis. Predictions will be compared with the experimental results of this work and the previous results of Jorgensen (3, 4).

THEORY

Wagner's Theory of Oxidation

Consider a metal which is placed in a furnace containing an oxidizing gas at elevated temperature. Assume that in this temperature range a coherent scaling layer is formed. Assume further that after a brief transient, growth of the scale becomes rate limited by steady state diffusion of ions or electrons through the scale. Thereafter the current due to ions must balance that due to electrons under open circuit conditions. Hence, as scaling proceeds, the net or total current flowing through the film vanishes. The physics of this scaling system have been treated previously by Wagner (26), and his treatment is summarized in block diagram form in Figure 2. Only the major hypotheses and results are presented in the figure; however, for a more detailed presentation see, for example, Hauffe (32) or Wagner (26).

The results of Wagner's theory are very useful for gaining insight concerning the nature of the diffusing species (defect structure) in a mixed conducting scale. By knowing E_W and the scaling rate constant, k, as functions of μ_{X_2}; i.e., nonmetal chemical potential, the ionic and electronic conductivities can also be determined as functions of μ_{X_2}. Alternatively, by knowing the μ_{X_2} dependences of the ionic and electronic conductivities of the scale material, the scaling rate constant of the metal can be predetermined. This knowledge also allows one to alter the scaling rate of a metal by doping to alter the concentration and, therefore, the conductivity of the rate

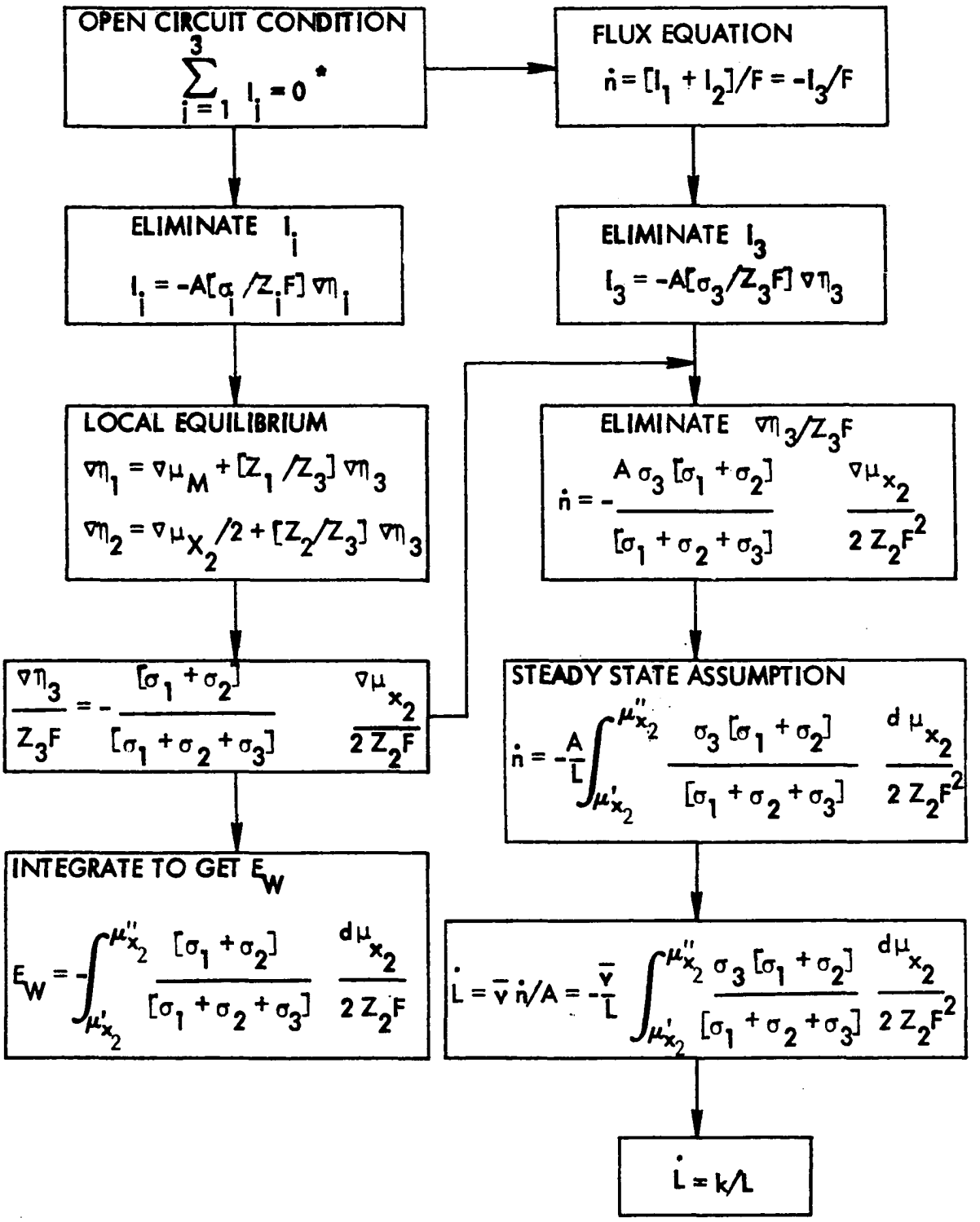

Figure 2. Derivation of the open circuit emf and scaling rate equations from Wagner's scaling rate theory (26).

controlling species. The results, hypotheses and implications of Wagner's theory have been tested by a large number of investigators over the past 40 years and have withstood the test of time.

Theory of Applied Electric Fields on Diffusion Controlled Scaling Kinetics

Wagner's theory of oxidation can be extended to include externally applied electric fields and the migration of uncharged defects by altering the boundary conditions and by incorporating an additional term for neutral transport in the basic flux equation. The flux equation may then be written as

$$\dot{n} = [I_1 + I_2]/F + 2z_2 A J_{X_2}/N \qquad [2]$$

where $\dot{n}$ is the rate of formation of the scale compound in equivalents/sec, I_1 and I_2 are, respectively, the cation and anion currents, J_{X_2} is the neutral flux (assumed here to be diatomic), z_2 is the valence of the anion species, and N is Avagadro's number. Equation [2] is identical to Wagner's flux equation except that a parallel flux of uncharged X_2 molecules has been inserted.

From the flux equation so modified an expression for $\dot{L}$ can be derived in a manner similar to that used by Wagner for the open circuit case. The main difference involves the use of more general boundary conditions in which the total current is allowed to differ from zero. Choudhury and Patterson (33) have recently presented an extension to Wagner's theory of mixed conduction in ionic solids (34)

in which the total current was considered to differ from zero. Equations were developed to evaluate the performance characteristics of solid electrolyte cells exhibiting mixed ionic and electronic conduction and invariant cell geometry. In the following derivation for $\dot{L}$ certain of the equations derived by Choudhury and Patterson are utilized; however, the assumption of constant cell geometry must now be relaxed. Because the scale thickening (or thinning) kinetics are sought, these equations must now be considered to vary with time. Rather than reconstruct the original derivations in detail, a summary is presented in block diagram form in Figure 3. Equations from this summary are used as the derivation for $\dot{L}$ progresses.

In the following analysis extensive use is made of the parameter r which is defined to be the sum of the ionic currents divided by the electronic current at each location in the scale. These currents are assumed constant throughout the scale (i.e., steady state). Thus, r is also independent of location in the scale, and many of the subsequent equations are in terms of this parameter. Although r cannot, in general, be measured experimentally, it is very useful to derive parametric equations in terms of this parameter. For example, parametric equations for the cell voltage and total current were cast in terms of r in Choudhury and Patterson's theoretical treatment of performance characteristics in solid electrolyte galvanic cells. Plots of cell voltage vs total current were generated by simply varying r. A solution to the differential equation for $\dot{L}$ is also greatly facilitated with the use of r in the present work. Equations for scale thickness, cell voltage, total current and time will be in terms of this parameter.

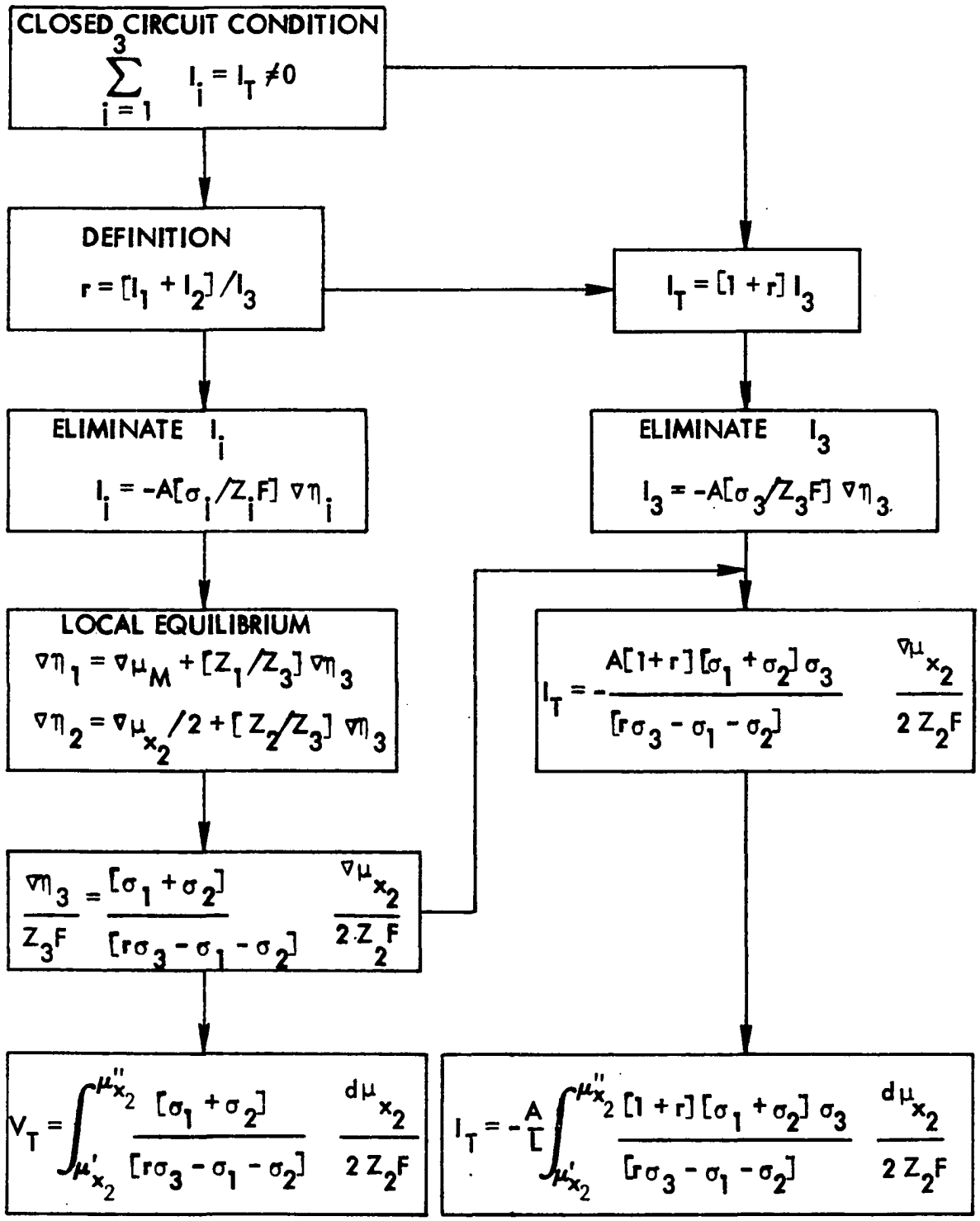

Figure 3. Derivation of the cell voltage and total current equations for a mixed conducting compound under steady state conditions (after Choudhury and Patterson, reference 33).

The total current I_T through the scale vanishes for Wagner's open circuit case (26). However,

$$I_T = I_1 + I_2 + I_3 \neq 0 \qquad [3]$$

in the present case where I_3 is the electronic current. Substituting Eq. [3] into [2] we get

$$\dot{n} = I_T/F - I_3/F + 2z_2AJ_{X_2}/N. \qquad [4]$$

From Figure 3

$$I_3 = - A[\sigma_3/z_3F]\nabla\eta_3 \qquad [5]$$

where σ_3 is the local electronic conductivity, and η_3 is the electrochemical potential of electrons. The term η_3 can be eliminated (Figure 3) in favor of nonmetal chemical potential by using

$$\frac{\nabla\eta_3}{z_3F} = \frac{[\sigma_1 + \sigma_2]}{[r\sigma_3 - \sigma_1 - \sigma_2]} \frac{\nabla\mu_{X_2}}{2z_2F} \qquad [6]$$

where σ_1 and σ_2 are, respectively, the local cation and anion conductivity. Substituting Eq. [6] into [5] we get

$$I_3 = - \frac{A\sigma_3[\sigma_1 + \sigma_2]}{[r\sigma_3 - \sigma_1 - \sigma_2]} \frac{\nabla\mu_{X_2}}{2z_2F}, \qquad [7]$$

and Eq. [4] becomes

$$\dot{n} = I_T/F + \frac{A\sigma_3[\sigma_1 + \sigma_2]}{[r\sigma_3 - \sigma_1 - \sigma_2]} \frac{\nabla\mu_{X_2}}{2z_2F^2} + 2z_2AJ_{X_2}/N. \qquad [8]$$

By letting $J_{X_2} = - D_{X_2}\nabla C_{X_2}$, integrating over the scale thickness and then dividing by L we get

$$\dot{n} = I_T/F + \frac{A}{L}\left\{\int_{\mu'_{X_2}}^{\mu''_{X_2}} \frac{\sigma_3[\sigma_1 + \sigma_2]}{[r\sigma_3 - \sigma_1 - \sigma_2]} \frac{d\mu_{X_2}}{2z_2F^2} - 2z_2D_{X_2}\Delta C_{X_2}/N\right\} \quad [9]$$

where ΔC_{X_2} is the difference in concentration of neutral species across the scale and D_{X_2} is the diffusivity of the neutral species. The rate of scale thickening assuming planar growth is given by

$$\dot{L} = \bar{v}\dot{n}/A. \quad [10]$$

Eliminating $\dot{n}$ between Eqs. [9] and [10] yields

$$\dot{L} = \frac{\bar{v}I_T}{FA} + \frac{\bar{v}}{L}\left\{\int_{\mu'_{X_2}}^{\mu''_{X_2}} \frac{\sigma_3[\sigma_1 + \sigma_2]}{[r\sigma_3 - \sigma_1 - \sigma_2]} \frac{d\mu_{X_2}}{2z_2F^2} - 2z_2D_{X_2}\Delta C_{X_2}/N\right\}, \quad [11]$$

or more simply

$$\dot{L} = \frac{\bar{v}I_T}{FA} + \frac{1}{L}\left[-k(r)/r + k_n\right] \quad [12]$$

where

$$k(r) = -\bar{v}\int_{\mu'_{X_2}}^{\mu''_{X_2}} \frac{r\sigma_3[\sigma_1 + \sigma_2]}{[r\sigma_3 - \sigma_1 - \sigma_2]} \frac{d\mu_{X_2}}{2z_2F^2}\ ;\ k_n = -2z_2\bar{v}D_{X_2}\Delta C_{X_2}/N. \quad [13]$$

Equation [12] is the general equation which predicts the effect of applied electric fields on diffusion controlled scaling kinetics.

Limiting cases

From Eq. [11] several limiting cases can be delineated which show that the present work embraces Wagner's treatments (26, 34) as

special cases. For example, when r = - 1; i.e., when $I_1 + I_2 = - I_3$, the total current is zero. If $J_{X_2} = 0$, Eq. [11] reduces to

$$\dot{L} = \frac{1}{L}\left\{-\bar{v}\int_{\mu'_{X_2}}^{\mu''_{X_2}} \frac{\sigma_3[\sigma_1 + \sigma_2]}{[\sigma_1 + \sigma_2 + \sigma_3]} \frac{d\mu_{X_2}}{2z_2F^2}\right\} = k/L, \qquad [14]$$

and it can be easily recognized that this expression is identical to the one derived by Wagner for the open circuit case where $I_T = 0$ (Figure 2).

Equation [6] may be integrated to give (Figure 3)

$$V_T = \int_{\mu'_{X_2}}^{\mu''_{X_2}} \frac{[\sigma_1 + \sigma_2]}{[r\sigma_3 - \sigma_1 - \sigma_2]} \frac{d\mu_{X_2}}{2z_2F} . \qquad [15]$$

Substitution of r = - 1 into this equation gives

$$V_T = -\int_{\mu'_{X_2}}^{\mu''_{X_2}} \frac{[\sigma_1 + \sigma_2]}{[\sigma_1 + \sigma_2 + \sigma_3]} \frac{d\mu_{X_2}}{2z_2F} = E_W \qquad [15a]$$

where it can be recognized from Figure 2 that V_T is identical to the emf, E_W, across a scale growing under open circuit conditions.

Another interesting limiting case occurs when J_{X_2} is again set equal to zero and r = 0. This condition occurs when the ionic current is blocked; i.e., $I_1 + I_2 = 0$ and corresponds to the case where scale growth has been arrested. Here $\dot{L}$ in Eq. [11] vanishes and

$$I_T = \frac{A}{L}\int_{\mu'_{X_2}}^{\mu''_{X_2}} \sigma_3 \frac{d\mu_{X_2}}{2z_2F} . \qquad [16]$$

This equation is identical to one derived by Wagner in a later paper (34) dealing with mixed conduction in ionic solids of fixed thickness. The total current is now due only to the migration of electrons under completely ion blocking or polarization conditions. Substituting r = 0 into Eq. [15] yields the following expression for the halt voltage, V_{Halt}:

$$V_T = V_{Halt} = - (\mu''_{X_2} - \mu'_{X_2})/2z_2F = E_{TH} \qquad [17]$$

where E_{TH} is the thermodynamic emf for the oxidation reaction. In other words the scaling process is completely arrested when a voltage equal and opposite to the thermodynamic emf is applied to the cell.

In the above limiting cases J_{X_2} was set equal to zero. If a parallel flux of neutral molecules (or atoms) through the scale exists, however, complications arise. For example, in the limiting case just mentioned, the parameter r was equal to zero when the scaling process became arrested. This is no longer true when a parallel flux of neutral molecules exists. In order to stop the scaling process in this case, an ionic current must still exist to decompose the scale being continuously formed due to the migration of X_2 molecules which are uninfluenced by applied electric fields. The magnitude of this current is proportional to J_{X_2}.

A quantitative expression for V_{Halt} in this case may be obtained by setting $\dot{n}$ in Eq. [2] equal to zero and substituting the appropriate expressions for I_1 and I_2 (Figure 2). Whence,

$$- 2z_2FAJ_{X_2}/N = I_1 + I_2 = - A[\sigma_1/z_1F]\nabla\eta_1 - A[\sigma_2/z_2F]\nabla\eta_2 . \qquad [18]$$

Invoking the assumption of local equilibrium (Figure 2) we get

$$2z_2FJ_{X_2}/N = [\sigma_1 + \sigma_2] \frac{\nabla\mu_{X_2}}{2z_2F} + [\sigma_1 + \sigma_2] \frac{\nabla\eta_3}{z_3F} . \qquad [19]$$

Simplifying and integrating over the scale thickness we obtain

$$V_{Halt} = E_{TH} + \frac{2z_2FJ_{X_2}}{N} \int_0^L \frac{d\ell}{[\sigma_1 + \sigma_2]} . \qquad [20]$$

Thus, V_{Halt} is greater than E_{TH} by an amount proportional to the neutral flux. If the magnitude of J_{X_2} and the spatial dependences of σ_1 and σ_2 are known, the halt voltage can be calculated using Eq. [20]. Alternatively, if V_{Halt} and the spatial dependences of σ_1 and σ_2 are known, J_{X_2} can be calculated. Part of the Jorgensen-Raleigh controversy (3, 14, 15, 16) involved a discussion of the halt voltage. Jorgensen observed halt voltages on the order of the thermodynamic emf in his experiments (3, 4). He argued qualitatively that any V_{Halt} greater than E_{TH} would be due to neutral oxygen molecules. However, no quantitative expression for the halt voltage in terms of the neutral flux was presented. Presumably Eq. [20] might have been instrumental for resolving a number of points of conflict in that controversy.

In principle, essentially two experimental schemes may be used to verify the theoretical arguments just presented. These are the potentiostatic or constant voltage case, in which the current is monitored as the thickness changes with time, and the galvanostatic or constant current case, in which voltage measurements reflect the variance of scale thickness with time.

Potentiostatic scaling kinetics

Choudhury and Patterson (33) give the following equation for the total current (Figure 3)

$$I_T = -\frac{A}{L}\int_{\mu'_{X_2}}^{\mu''_{X_2}} \frac{[1 + r][\sigma_1 + \sigma_2]\sigma_3}{[r\sigma_3 - \sigma_1 - \sigma_2]} \frac{d\mu_{X_2}}{2z_2F} \qquad [21]$$

where now L on the right side is considered to be time dependent. Substituting this equation into Eq. [11] results in a major simplification in the expression for $\dot{L}$ as follows

$$\dot{L} = \frac{\bar{v}}{L}\int_{\mu'_{X_2}}^{\mu''_{X_2}} \frac{[1 + r][\sigma_1 + \sigma_2]\sigma_3}{[r\sigma_3 - \sigma_1 - \sigma_2]} \frac{d\mu_{X_2}}{2z_2F^2}$$

$$+ \frac{\bar{v}}{L}\int_{\mu'_{X_2}}^{\mu''_{X_2}} \frac{\sigma_3[\sigma_1 + \sigma_2]}{[r\sigma_3 - \sigma_1 - \sigma_2]} \frac{d\mu_{X_2}}{2z_2F^2} + \frac{k_n}{L} . \qquad [22]$$

Because r is independent of μ_{X_2} Eq. [22] may be written as

$$\dot{L} = [(\frac{1 + r}{r})k(r) - (\frac{1}{r})k(r) + k_n]/L, \qquad [23]$$

which can be simplified to give

$$\dot{L} = [k(r) + k_n]/L. \qquad [24]$$

Integration of Eq. [24] yields the relation

$$L^2 = L_0^2 + 2[k(r) + k_n][t - t_0] \qquad [25]$$

where k(r) and k_n are given by Eq. [13]. From Eq. [24] and [13] it can be seen that parabolic kinetics should result whenever the parameter r is independent of time.

Significantly, Eq. [15] indicates that r must be constant when V_T is invariant with time since the limits of integration, μ'_{X_2} and μ''_{X_2}, are fixed. Therefore, applying a constant voltage to the cell will cause the scale to grow or decompose parabolically at a rate determined by the transport parameters (σ_1, σ_2 and σ_3) of the scale.

Since the voltage is held constant and the film thickness is changing with time, i.e., the cell resistance is changing with time, the current flowing through the scale must also be time dependent. The kinetics should, therefore, be observable in situ by monitoring the cell current with time. The relationship between current and time can be derived by writing Eq. [21] as

$$L = [\frac{AF}{\bar{V}} (\frac{1 + r}{r})k(r)]/I_T \qquad [26]$$

or

$$L^2 = [\frac{AF}{\bar{V}} (\frac{1 + r}{r})k(r)]^2/I_T^2 . \qquad [27]$$

Substituting Eq. [27] into [25] results in an equation of the form

$$I_T^{-2} = K_1 + K_2[t - t_0] \qquad [28]$$

where

$$K_1 = [\frac{AF}{\bar{V}} (\frac{1 + r}{r})k(r)]^{-2}L_0^2; \quad K_2 = 2[\frac{AF}{\bar{V}} (\frac{1 + r}{r})k(r)]^{-2}[k(r) + k_n]. \qquad [29]$$

A plot of I_T^{-2} vs $t - t_0$ results in a straight line of slope K_2 and intercept K_1.

It should be remembered that Eq. [25] and [28] were derived with no particular assumptions on defect structure or transport models in the scale. Therefore, the parabolic scaling kinetics indicated in Eq. [25] and [28] may be expected in potentiostatic experiments independent of defect structure. Experiments involving scales of widely different defect structures should differ only in the values of K_1 and K_2 which result but not in the kinetics. Combining defect structure hypotheses with values of k_n, r and the conductivity parameters, allows prediction of the empirical parameters K_1 and K_2.

Galvanostatic scaling kinetics

One of the major goals of this work is to compare Jorgensen's experimental results (3, 4) with the theoretical predictions presented in this work. His experiments were run under constant current conditions and yielded plots of thickness and voltage as functions of time. Hence, expressions will now be derived for the time dependences of L and V_T for the galvanostatic case. Since V_T now changes with time, it is apparent from Eq. [15] that r and, hence, k(r) must also vary with time. Accordingly Eq. [24] can no longer lead to a parabolic time dependence for L(t) because it is now of the form

$$\dot{L} = \frac{1}{L}\left[k(r, t) + k_n\right]. \qquad [30]$$

Equation [30] is not readily solved to give the time dependence of L, and only indirect and laborious techniques can now be used.

In order to obtain the scaling kinetics in this case, it is necessary to first obtain an expression for the time dependence of r. Once that is done, the time dependences of V_T and L can be calculated from the bottom two formulas in Figure 3. In what follows parametric equations for t, V_T and L will be derived in terms of the parameter r so that t, V_T and L can be obtained as functions of each other.

A derivation for obtaining the general solution for t = t(r) is presented in Appendix A. There it is shown that r and $t - t_0$ are implicitly related by a formula of the type

$$[A\text{-}8] \qquad t - t_0 = \int_{r_0}^{r} A(r)/B(r)dr$$

where A(r) and B(r) are very cumbersome integral functions of r and the transport parameters of the scale but are not explicitly dependent on t. In principle Eq. [A-8] can be used without any special assumptions about defect structure by just leaving the expressions for A(r) and B(r) in terms of partial ionic and electronic conductivities. Efforts to retain this level of generality, however, result in highly intractable mathematical formulas which are difficult to interpret. Alternatively, specialized semi-empirical formulas for the partial conductivities may be used to advantage early in the analysis. Of course some generality is sacrificed in doing this; however, the mathematics become somewhat more manageable. This latter approach will be used in the present work.

A survey of previously reported conductivity studies for numerous scaling compounds at elevated temperatures indicates that a large number of scaling layers can be classified into one of two general

ionic defect models (23). These are the constant ionic conductivity model which applies to predominantly ionic conducting scales and the constant ionic transference number model which applies to predominantly electronic conducting scales. Techniques for deriving the galvanostatic scaling kinetics for these two models will now be outlined. Complete derivations are presented in the appendices.

Scaling kinetics for the constant ionic conductivity model

Many scaling layers are known to be predominantly ionic conductors over a significant range of μ_{X_2}. Included in this class are the lead (35, 36), silver (37, 38) and cuprous (39, 40) halides together with calcium fluoride (41), thorium dioxide (42) and probably a host of other scale compounds. These scales exhibit an ionic conductivity that is independent of μ_{X_2} in contrast to their electronic conductivities which typically vary as $P_{X_2}^{\pm 1/n}$.

The constant ionic conductivity model allows us to make considerable simplifications in the analysis presented in Appendix A. A detailed derivation of the scaling kinetics assuming the constant σ_{ion} model is presented in Appendix B, and an example is given for the kinetics of silver bromination under galvanostatic conditions. Although the detailed derivations are crucial for the development, they have been placed in the appendices. This was done only to improve the clarity and continuity of the text and does not in any way imply that they are unimportant. Only the major results are cited here, and the reader is referred to Appendix B for the details.

The following expression is derived for the time dependence of r in Appendix B:

$$[B\text{-}8] \qquad t - t_0 = \int_{r_0}^{r} \frac{\varphi\Delta d(\varphi\Delta)}{a + b\Delta}$$

where

$$[B\text{-}7] \qquad \varphi = \left(\frac{1 + r}{r}\right); \ \Delta = E_{TH} - V_T; \ a = \left[\frac{I_T}{\sigma_{ion} A}\right]^2 k_n; \ b = \frac{\bar{v}}{\sigma_{ion} F}\left[\frac{I_T}{A}\right]^2 .$$

Equation [B-8] cannot be simplified further if k_n is nonzero, and numerical techniques must be used to solve this equation when the appropriate expressions (see Eq. [B-7]) for φ, Δ, a and b are inserted. If k_n is zero, as is the case for silver bromide, Eq. [B-8] can be further simplified to give

$$[B\text{-}10] \qquad 2b[t - t_0] = \varphi^2\Delta \Big|_{r_0}^{r} + \int_{r_0}^{r} \varphi^2 d\Delta .$$

This equation can be solved exactly when the appropriate expressions for φ and Δ are inserted. The expression for Δ; i.e., $(E_{TH} - V_T)$ is dependent upon the particular defect structure of the scale compound under consideration.

The silver bromination system is used as a particular example to show how Eq. [B-10] may be integrated to give t = t(r). The final result is that

$$t - t_0 = \frac{RT}{2bF}\left\{\left[\left(\frac{1 + r}{r}\right)^2 + 1\right]\ell n\left[\frac{1 - r\beta}{1 - r\alpha}\right] + [2\beta + \beta^2]\,\ell n\left[\frac{1 - r\beta}{r}\right]\right.$$

$$[B\text{-}17] \qquad \left. + [2\alpha + \alpha^2]\,\ell n\left[\frac{1 - r\alpha}{r}\right] + \left[\frac{\beta - \alpha}{r}\right]\right\}_{r_0}^{r}$$

where $\alpha = (P'_{Br_2}/P_{\oplus})^{1/2}$, $\beta = (P''_{Br_2}/P_{\oplus})^{1/2}$ and r_0 is the initial steady state value of r set up when the current is applied. $P_{\oplus}$ is the bromine pressure at which the ionic and hole conductivities are equal. Although Eq. [B-17] is a simplification over Eq. [A-8], it is itself rather cumbersome. Nevertheless, it is in closed form and can be used to interpolate the value of r at any time t desired. In principle equations similar to Eq. [B-17] can be obtained for any scaling system for which the constant ionic conductivity model is valid for the scale and for which k_n is negligible. Only expressions for Δ and $d\Delta$ will change depending upon the particular defect structure.

The procedure for obtaining the scaling kinetics assuming galvanostatic conditions and the constant σ_{ion} model of Appendix B can be summarized as follows: 1) Determine the magnitudes and P_{X_2} dependences of the conductivity parameters which are used to obtain an expression for Δ. 2) Determine r_0 for a given set of experimental conditions; namely, I_T and L_0. 3) Increment r from r_0 to any desired final value. 4) Calculate the corresponding values of $t - t_0$, V_T and L from Eqs. [B-17], [15] and [B-3] which are all parametric in r. 5) One may then plot L and V_T versus the calculated values of $t - t_0$. In this way the galvanostatic scaling kinetics for any given set of experimental conditions can be predicted quantitatively. Accelerated growth will be predicted when $r < -1$ or $V_T < E_W$; retarded growth when $-1 < r < 0 + \delta$ or $E_W < V_T < V_{Halt}$ and decomposition or scale thinning when $r > 0 + \delta$ or $V_T > V_{Halt}$. The quantity δ is an indication of the amount of neutral transport through the scale, and if $\delta = 0$; $V_{Halt} = E_{TH}$.

Scaling kinetics for the constant ionic transference number model The second special case to be considered is the constant ionic transference number, t_{ion}, model. Many scaling layers are known to be predominantly electronic conductors. Generally these scaling layers possess a μ_{X_2} independent ionic transference number. Several of these materials are ZnO, Cu_2O, NiO, Cr_2O_3, CdO, etc. (23, 32). A treatment similar to that outlined in the previous section could be presented here for the constant t_{ion} model. Again, an expression could be derived for $t = t(r)$ from which V_T and L as functions of $t = t_0$ could be deduced just as before. Fortunately, however, t_{ion} is now independent of μ_{X_2}, and a greatly simplified version of Eq. [11] results from which the kinetic equations may be derived. Again, only the important results are exploited here in the text while the detailed derivations for this case are given in Appendix C.

The following alternative equation to Eq. [11] is derived in the appendix

$$[C\text{-}5] \qquad \dot{L} = \frac{\bar{v} I_T}{FLA} \int_0^L t_{ion} d\ell + [k + k_n]/L$$

where it is also shown that this equation reduces identically to Eq. [11]. Equation [C-5] is virtually equivalent to Eq. [1] derived by Kröger (23). As was mentioned earlier, such equations are not useful for all cases involving galvanostatic scaling kinetics or even for the constant ionic conductivity case. This is because the spatial integral from 0 to L can, in general, be time dependent thereby greatly complicating the differential equation.

The integral in Eq. [C-15] is greatly simplified, however, for the constant t_{ion} case because t_{ion} does not depend explicitly on location in the scale or on time. Under these assumptions one obtains (see Appendix C) the following equation for the time dependence of L

$$[C\text{-}7] \qquad t - t_0 = \frac{1}{c}\left\{L - L_0 + L_\infty \ell n\left[\frac{L_\infty - L}{L_\infty - L_0}\right]\right\}$$

where the constant c, the rate of electrolysis of the scale, is proportional to I_T. L is the final or steady state thickness of the scale which occurs when the electrolysis rate just balances the diffusional fluxes. As is shown in Appendix C, L_∞ is given by $-[k + k_n]/c$.

If L and L_0 are sufficiently less than L_∞, parabolic kinetics are predicted. This indicates that the electrolysis term has little effect on the scaling kinetics in this thickness range. On the other hand, linear kinetics are predicted by Eq. [C-7] when L and L_0 are much greater than L_∞. In this regime thickness increases or decreases linearly with time depending on the sign of I_T in the electrolysis term. In general, Eq. [C-7] will predict accelerated growth, retarded growth or thinning of the scaling layer depending on the magnitude and polarity of the electrolysis term, c.

In order to obtain the time dependence of the voltage, an alternate form of Eq. [15] is derived because the time dependence of r is unknown in this case. The expression for V_T in terms of L is given in Appendix C as

$$[C\text{-}9] \qquad V_T = E_W - \frac{I_T}{A}\int_0^L \frac{\cdots\, d\ell \,\cdots}{[\sigma_1 + \sigma_2 + \sigma_3]} \,.$$

Again this equation is only useful for the constant t_{ion} model. For the general case, as well as the constant ionic conductivity case, the integral in Eq. [C-9] is dependent on the parameter r which can vary with time. For the constant t_{ion} model the integral on ℓ is independent of r as is also shown in Appendix C, and Eq. [C-9] becomes

$$[C\text{-}19] \qquad V_T = E_W - \frac{I_T L}{\bar{\sigma}_T A}$$

where

$$[C\text{-}20] \qquad \bar{\sigma}_T = - \frac{nRT\sigma_T^o(\Delta P_{X_2}^{1/n})}{2z_2 F E_{TH}} ,$$

σ_T^o being the sum of the ionic and electronic conductivities at P_{X_2} = 1 atm. It can be seen from Eq. [C-19] that V_T is proportional to L so that once we deduce the relation between L and t from Eq. [C-7], we may interpolate to generate a plot or table of V_T values versus $t - t_0$. Thus, Eqs. [C-7] and [C-19] are useful for analyzing galvanostatic kinetics of a scaling layer whose ionic transference number is independent of μ_{X_2} (or P_{X_2}).

Summary of the theoretical section

A quantitative theory for the effect of applied electric fields on diffusion controlled scaling kinetics was presented. A formula (Eq. [11]) was derived for $\dot{L}$ in terms of I_T, r, k_n and the conductivity parameters of the scaling layer. It was shown that Wagner's scaling rate theory (26) is a special case of the present, more, general treatment. A quantitative expression for the halt voltage was derived

(Eq. [20]) which would be useful in assessing the amount of neutral transport in scaling layers.

The differential equation (Eq. [11]) describing the growth kinetics was solved for two useful experimental cases; namely the potentiostatic and galvanostatic cases. This equation for $\dot{L}$ may be solved without any assumptions on defect equilibria within the scaling layer for the potentiostatic scaling kinetics, and parabolic growth kinetics always result. Plots of L^2 versus $t - t_0$ and I_T^{-2} versus $t - t_0$ give straight lines whose slopes and intercepts may be readily interpreted.

The differential equation for $\dot{L}$ is not easily solved for galvanostatic scaling kinetics. This is because the parameter r is time dependent. General solutions as well as more specialized solutions to the differential equation of scale thickening or thinning require that the time dependence of r must first be deduced. In general, this time dependence is not readily obtained, and therefore, special case solutions were derived.

It should be emphasized that the foregoing theoretical development, with its highly definitive and quantitative formulas, constitutes perhaps the most important contribution of the present work. Not until formulas of this sort are developed can one truly scrutinize the applicability of any theory to practical or experimental situations. Indeed it will be shown below that Wagner's concepts of parabolic scaling kinetics, when properly modified for nonopen circuit conditions, are not sufficient to describe the effects observed in this work and in previous studies (3, 4). This position is in sharp

contrast to that held by other authors who have argued mainly on qualitative grounds (3-5, 14-16, 25). Had the logical consequences of Wagner's concepts not been developed in terms of definitive quantitative formulas, the important discrepancies between theory and experiment would not have been brought into focus.

EXPERIMENTAL

In order to test the hypotheses presented in the previous section, two scaling systems were studied; namely, Ag, AgBr and Si,SiO_2. The Ag, AgBr scaling system was selected because, in principle, it should behave ideally. The defect transport mechanisms are well known for AgBr, and conductivity data are available as a function of μ_{Br_2} so that computer calculations predicting the effect of applied electric fields on silver bromination can be made. These predictions can in turn be compared with experimental results. The Si,SiO_2 system, as was mentioned earlier, was selected in order to resolve the Jorgensen-Raleigh controversy (3, 14-16) and to perhaps elucidate the mechanism of oxygen transport in SiO_2.

Silver Bromination

Apparatus

A schematic diagram of the apparatus used in the silver bromination study is shown in Figure 4. By using the pyrex stopcock and bubbler arrangement shown on the right hand side of the figure, the system could be pumped to a roughing pump vacuum, purged with helium or exposed to bromine with helium serving as the carrier gas. This gas was subsequently dried over a mixture of anhydrous magnesium perchlorate and anhydrous calcium sulfate. The KOH bubbler shown on the left hand side of the figure served to neutralize the effluent bromine vapor. Fluorolube halogen resistant stopcock grease (Hooker Chemical Corporation) was used on all ground glass joints.

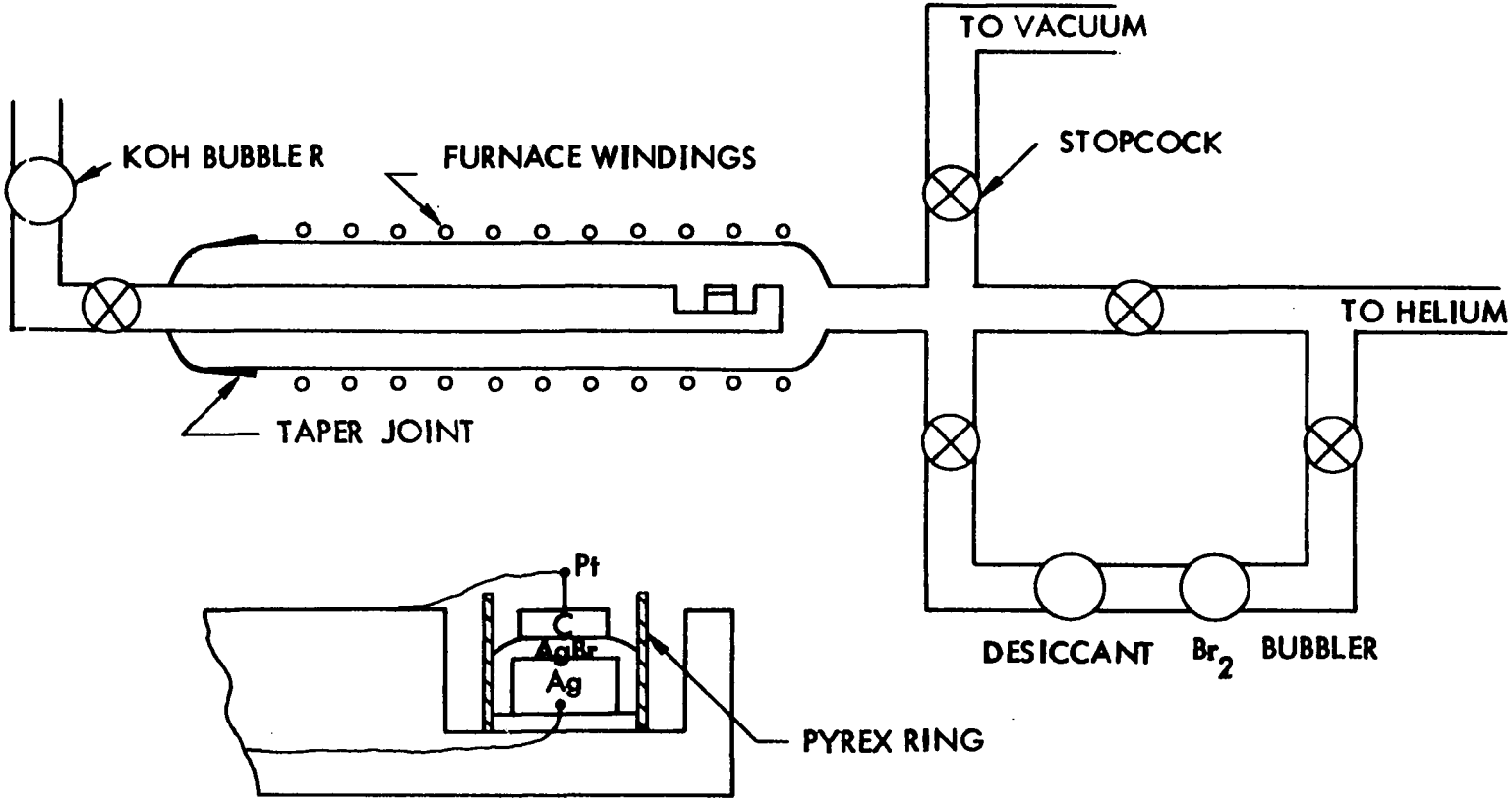

Figure 4. Schematic diagram of the apparatus and cell arrangement used in the silver bromination experiments.

The silver bromination cell was loaded into a pyrex cell holder, and this in turn was inserted into a pyrex furnace tube. The cell arrangement is shown in the insert in Figure 4. The platinum wires connected to the cell were insulated with small diameter pyrex tubing. The leads were brought out of the furnace tube with tungsten to pyrex seals. The cell temperature was determined with the use of a Pt,Pt-10% Rh thermocouple which had been calibrated with the melting points of lead and tin. Temperature control was to within $\pm$ 0.5 degree for each experiment.

Materials

The silver specimens used in this study were made by melting 20 gage silver wire (purity 99.8%) in a fused quartz crucible in air. The disks that were formed were approximately 1/4 inch thick by 5/8 inch diameter. After they were cast, their planar interfaces were mechanically ground and polished.

Reagent grade bromine was evolved into a flowing stream of helium by means of a bubbler at 0 ^{o}C with an ice bath. This temperature fixes a bromine partial pressure in the system of 0.083 atm (43).

Ultra pure graphite disks 1/8 inch thick and 1/2 inch in diameter and weighing less than 0.15 gram were used as the external electrodes on the AgBr scale.

Cell construction

Bromination cells were constructed in the following steps: A hole approximately 0.040 inch in diameter was drilled part of the way into one of the planar interfaces of the silver disk, and a platinum

wire containing a bead on the end was pressed into the hole. This specimen was loaded into the cell holder and inserted into the furnace tube. The specimen was subsequently pre-brominated at elevated temperature for a known length of time in order to establish a well defined initial thickness of AgBr according to the scaling rate data of Wagner (44). The cell holder was removed from the furnace tube and the graphite electrode containing a platinum wire lead was placed gently on the specimen. Welds were made to the two leads so that the final cell assembly appeared as shown in the insert in Figure 4.

Silicon Oxidation

Apparatus

Electrical measurements were made on silicon oxidation cells (A) situated on the cell support shown in Figure 5. The entire assembly was mounted in the vertical position so that the furnace could be raised or lowered over the furnace tube to rapidly heat and cool the cell. The O-ring, spacer, clamp arrangement (F, H, E) shown in the figure provided a gas tight seal to the fused quartz furnace tube (D).

The oxygen and helium gases used in this study were dried by passage over anhydrous magnesium perchlorate with anhydrous calcium sulfate as an indicator. The gas was admitted into the system through the inner tube (J) of the port (I) shown in the figure. It was then passed over the cell through holes in the alumina support plate (B) and discharged through the annular orifice (I).

Figure 5. Schematic diagram of the furnace tube support and cell assembly used in the silicon oxidation experiments.

(A) cell assembly

(B) alumina cell support plate

(C) alumina cell support tube

(D) fused quartz furnace tube

(E) brass clamp

(F) O-ring

(G) brass furnace tube support

(H) brass spacer

(I) gas outlet

(J) gas inlet

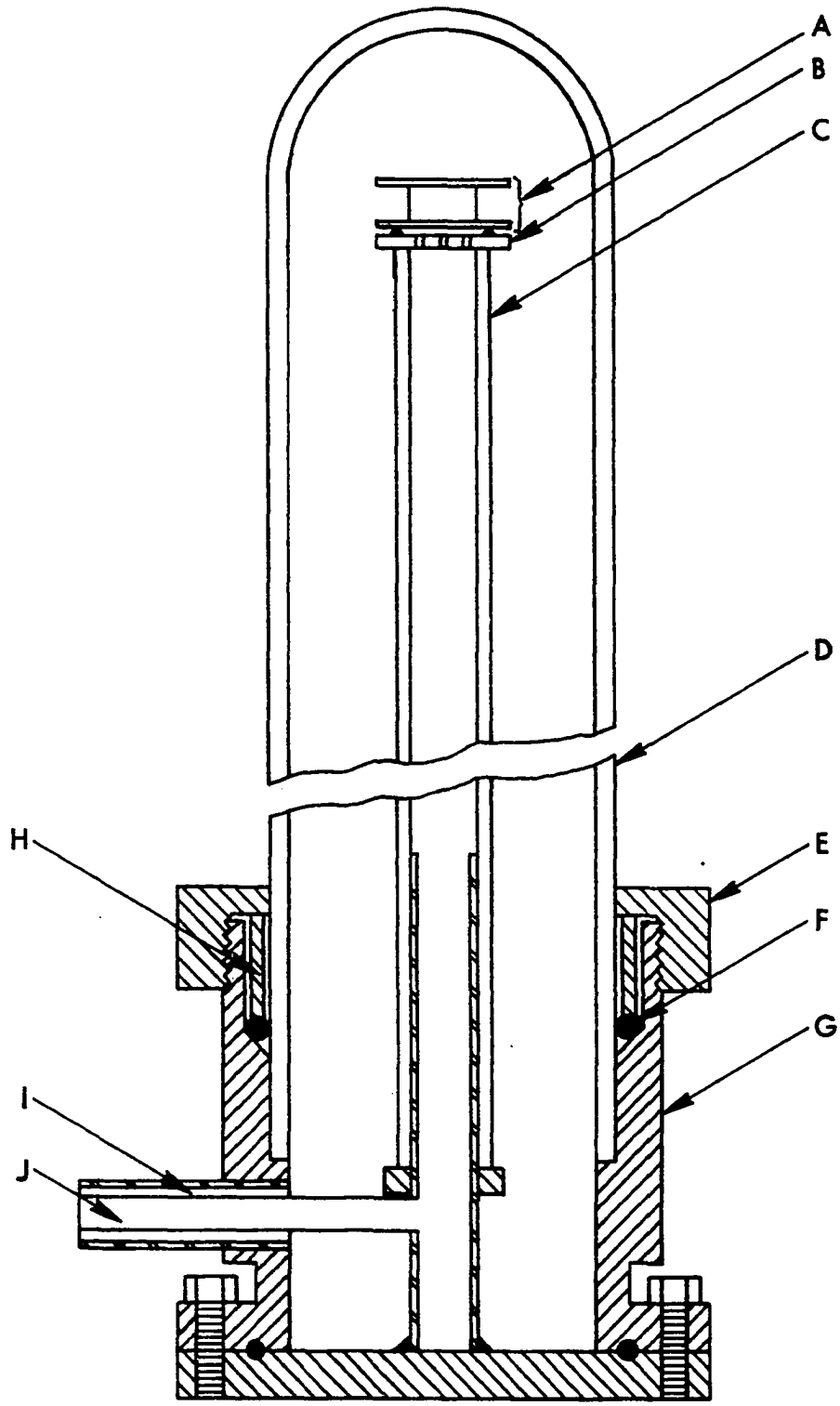
A
B
C
D
E
F
G
H
I
J

A high purity alumina tube (C) supported the cell in the hot zone of the furnace. Cell temperatures were measured with a Pt,Pt-10% Rh thermocouple which had been calibrated against the melting point of silver. Temperature control was to within $\pm$ 0.5 degree for a given experiment and $\pm$ 1.0 degree for the entire series of experiments.

Platinum wire leads (not shown in the figure) were connected to the cell and cell leads were protected with high purity alumina insulating tubing. The leads were brought out of the system through the use of an octal electrical feedthrough, and shielded copper wire was used for connections between the output terminals of the feedthrough and the instrument panel.

Constant voltages and currents were applied to the silicon oxidation cells through the use of the operational amplifier circuitry shown in Figure 6. In Figure 6a operational amplifier #II serves as a nonparasitic current measuring device, i.e., no ammeter is located in the circuit across which an IR drop would occur.

Materials

Ultra high purity high resistivity (1000 ohm cm) silicon was used in this study compliments of John Baker of Dow Corning Corporation. The single crystal disks were 1/4 inch thick by approximately 1/2 inch in diameter with the plane faces parallel to the (111) crystallographic plane. The disks had been electrochemically polished to a mirror finish.

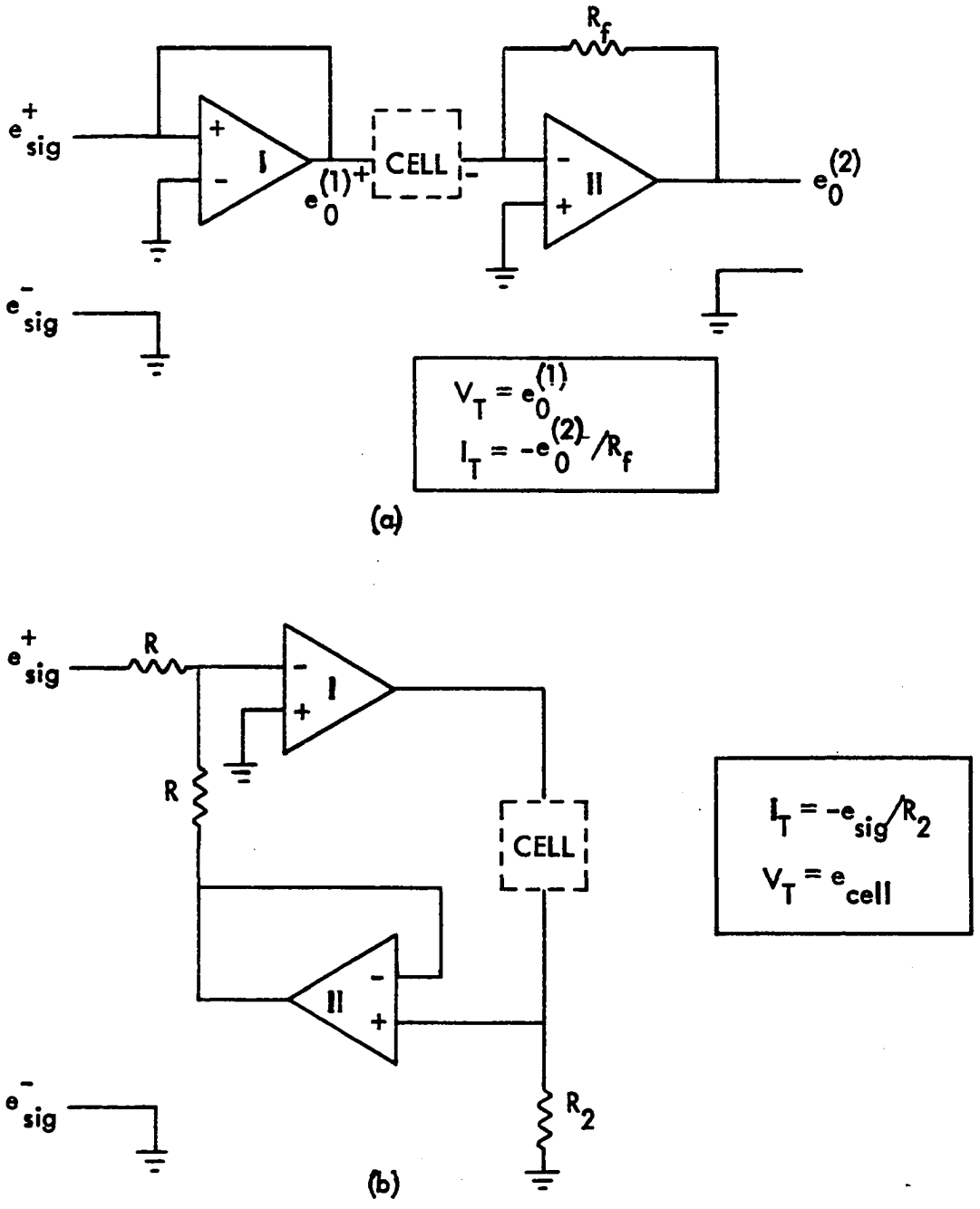

Figure 6. Operational amplifier circuitry used in the silicon oxidation experiments. a) Potentiostat with $R_f = 10^5$ ohm. b) Galvanostat with $R_2 = 10^6$ ohm.

Oxygen gas (purity 99.6%) was purified in the manner previously mentioned. All oxidation experiments were run at one atmosphere oxygen pressure.

Platinum electrodes were electron beam evaporated with the assistance of Frederick Schmidt of the Ames Laboratory and Jon Schieltz of Tektronix, Incorporated. These electrodes were approximately 1000 Å thick. Several specimens were also sent to Joseph Singer of NASA Lewis Research Center where platinum electrodes were sputtered onto the faces of the pre-oxidized specimens. These latter electrodes were approximately 300 Å thick.

Cell construction

The following procedure was used to clean the silicon disks before pre-oxidation. The specimens were ultrasonically cleaned for five minutes in each of the following reagents sequentially: trichloroethylene, methanol, distilled water, buffered hydrofluoric acid, distilled water, nitric acid and distilled water. This was followed by a five minute rinse in a jet of distilled water. The recipe for the buffered HF solution was offered by Joseph Brown of the Electrical Engineering Department and consisted of 90 g of ammonium bifluoride, 35 g of ammonium hydroxide and 300 g of distilled water. The specimens (usually four) were wiped dry with paper tissues and finally dried in a hot air stream. They were then loaded into the cell support and furnace tube shown in Figure 5, and the entire system was alternately pumped down to a roughing pump vacuum and flushed with helium several times. The final pump down cycle lasted

between one and twelve hours to remove traces of oxygen or water vapor in the gas phase. The system remained under vacuum during the heating cycle.

A tube furnace preheated to 850 ^{o}C was lowered over the system thereby rapidly heating the cell. Thermal equilibrium was generally reached in one hour, and the specimens were exposed to oxygen (P_{O_2} = 1 atm) for a given length of time depending upon the desired initial oxide film thickness. The oxide films formed in this manner were amorphous. The furnace was then lifted from the system, and the cell was cooled rapidly to room temperature.

Upon removal from the furnace tube, the specimens were observed under an optical microscope for defects. The initial oxide thickness, L_0, was determined with the use of optical interferometry. Holes approximately 0.040 inch in diameter were drilled into the edge of the silicon disks with a carbide drill. Since cutting oil was used in this operation, the specimens were re-cleaned by the technique mentioned earlier except that the HF cleaning operation was deleted.

The platinum electrodes mentioned earlier were applied to each face of the specimen. These electrodes are porous to oxygen gas at elevated temperatures. The porous nature of the electrodes is shown in Figure 7. Platinum was chosen over other noble metals such as silver and gold because it does not diffuse into the SiO_2. Silver and gold are known to diffuse into SiO_2 under the influence of applied electric fields (45).

For the final operations in the cell construction, a platinum wire containing a bead on the end was pressed into the hole on the

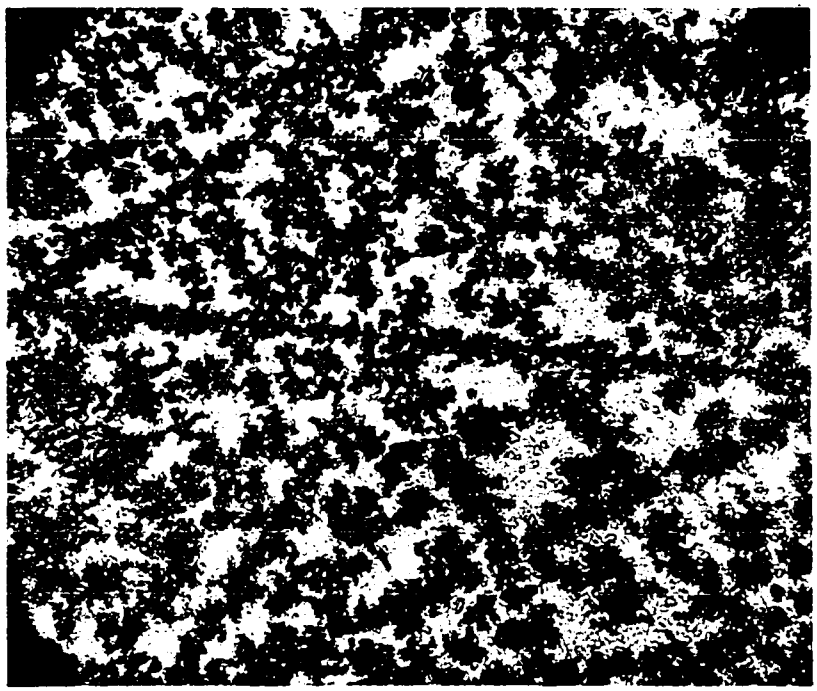

(a)

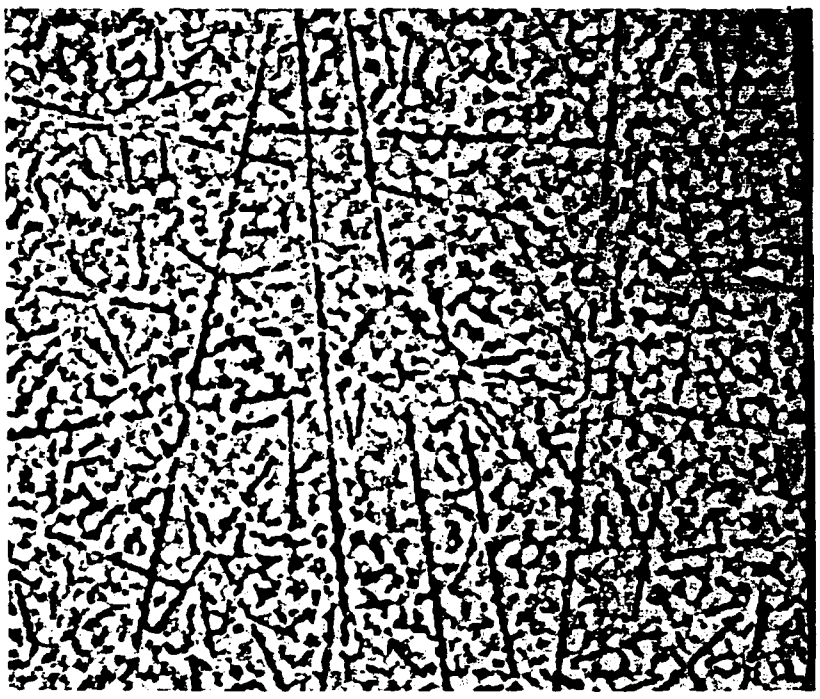

(b)

Figure 7. Photomicrographs of a Pt/SiO_2 interface taken after an applied electric field experiment. The porous nature of the platinum electrodes is apparent. a) Optical micrograph (X 250). b) SEM micrograph (X 1500). Light regions of the micrographs are the platinum. Dark regions are the SiO_2.

edge of the specimen. The cell was then placed between two foils of platinum on the cell support (Figure 5), and electrical leads were attached.

During all of the operations described above, extreme care was taken to avoid contacting the specimens with the fingers to safeguard against sodium contamination. SiO_2 has an extremely small intrinsic conductivity due to oxygen at elevated temperatures, and minute traces of alkali-, aluminum-, hydroxyl- and hydrogen ions can contribute significantly to the conductivity. Significant alterations in the oxidation rate of silicon would be expected with this impurity doping (46).

RESULTS AND DISCUSSION

Silver Bromination

Applied electric field experiments

Bromination cells, constructed in the manner described earlier, were studied at temperatures in the range 200 to 350 °C. The cells were exposed to bromine gas with P_{Br_2} = 0.083 atm and $P_{He} + P_{Br_2}$ = 1 atm. The open circuit emf, E_W, was monitored with time until a steady state value was reached. Then constant currents and constant voltages were applied to the cell. This study consisted only of decomposition and acceleration experiments. Retarded bromination experiments were not conducted for the following reason. For this case cell voltages must be greater than E_W and less than E_{TH}. For silver bromide scaling layers E_W and E_{TH} are so close (37, 38) that little change in cell voltage or total current can be expected with time.

Decomposition experiments A total of four experiments were run in which the decomposition of AgBr was studied. Two of these experiments were conducted under potentiostatic conditions in which voltages large enough to decompose the AgBr scale were applied ($V_T > E_{TH}$). The current was monitored with time; however, the theoretically expected smooth traces in which the current increases parabolically with time were not observed. Instead very noisy traces were exhibited in which the current fluctuated sporadically between 1×10^{-4} and 0.75 amp. The time interval between fluctuations was typically on the order of a few seconds to several minutes. The erratic nature of these fluctuations suggested

that some sort of instability was acting to short circuit the cell. The following explanation is proposed.

When a voltage greater than the decomposition potential of AgBr is applied to the cell, silver bromide is decomposed at the anode (i.e., the AgBr, Br_2 interface) according to the reactions

$$h + AgBr \rightarrow \frac{1}{2} Br_2(g) + Ag_i^{\cdot} \qquad \text{for interstitials} \qquad [31]$$

and

$$h + AgBr + V'_{Ag} \rightarrow \frac{1}{2} Br_2(g) + Ag^{x}_{Ag} \qquad \text{for vacancies} \qquad [32]$$

where h is a positive hole, $Ag_i^{\cdot}$ is a silver ion interstitial, Ag^{x}_{Ag} is a silver ion on the silver ion sublattice and V'_{Ag} is a vacancy on the silver ion sublattice in accordance with the notation of Kröger and Vink (47).

At the cathode (Ag, AgBr interface) the following reactions advance to the right

$$Ag_i^{\cdot} \rightarrow Ag^{o} + h \qquad \text{for interstitials} \qquad [33]$$

and

$$Ag^{x}_{Ag} \rightarrow Ag^{o} + h + V'_{Ag} \qquad \text{for vacancies} \qquad [34]$$

where Ag^{o} is metallic silver in the standard state. The overall reaction becomes

$$AgBr \rightarrow \frac{1}{2} Br_2(g) + Ag^{o} \qquad [35]$$

which corresponds to net decomposition. In the theoretical arguments presented earlier, planar scale interfaces were assumed. Thus, for the case of decomposition, silver metal is assumed to be deposited

atom by atom in a planar array at the Ag, AgBr interface as shown in Figure 8a. However, if small instabilities should form by chance, as shown in Figure 8b, their growth will be favored according to simple laws of diffusion because the diffusion path is smaller from the anode to the tip of the instability than it is to the trailing planar interface. The largest instability will break away from the others as shown in Figure 8c and eventually forms a silver filament or dendrite which shorts the cell.

An interesting phenomenon occurs when this silver dendrite reaches the anode (Figure 8d). The cell is now short circuited causing an abrupt rise in the applied current. However, the dendrite tip is now directly exposed to Br_2 gas and hence, becomes rapidly brominated breaking the short circuit. As soon as the short circuit is broken, however, the decomposition voltage is restored across the cell. The cycle now repeats indefinitely causing the same observed erratic behavior. Apparently the other instabilities (i.e., those which lagged behind the first) experience net growth (Figure 8e) during the time intervals when the short circuit is broken because the electrolyzed AgBr scales were found to contain many extended dendrites of silver as will be described later.

This proposal could certainly account for the current fluctuations of four orders of magnitude observed during the AgBr decomposition experiments. Direct observations of the scales were undertaken to confirm the existence of the dendrites. The cells were cooled to room temperature while maintaining the voltage across the cell. The AgBr film was removed from the silver by simply melting the AgBr in

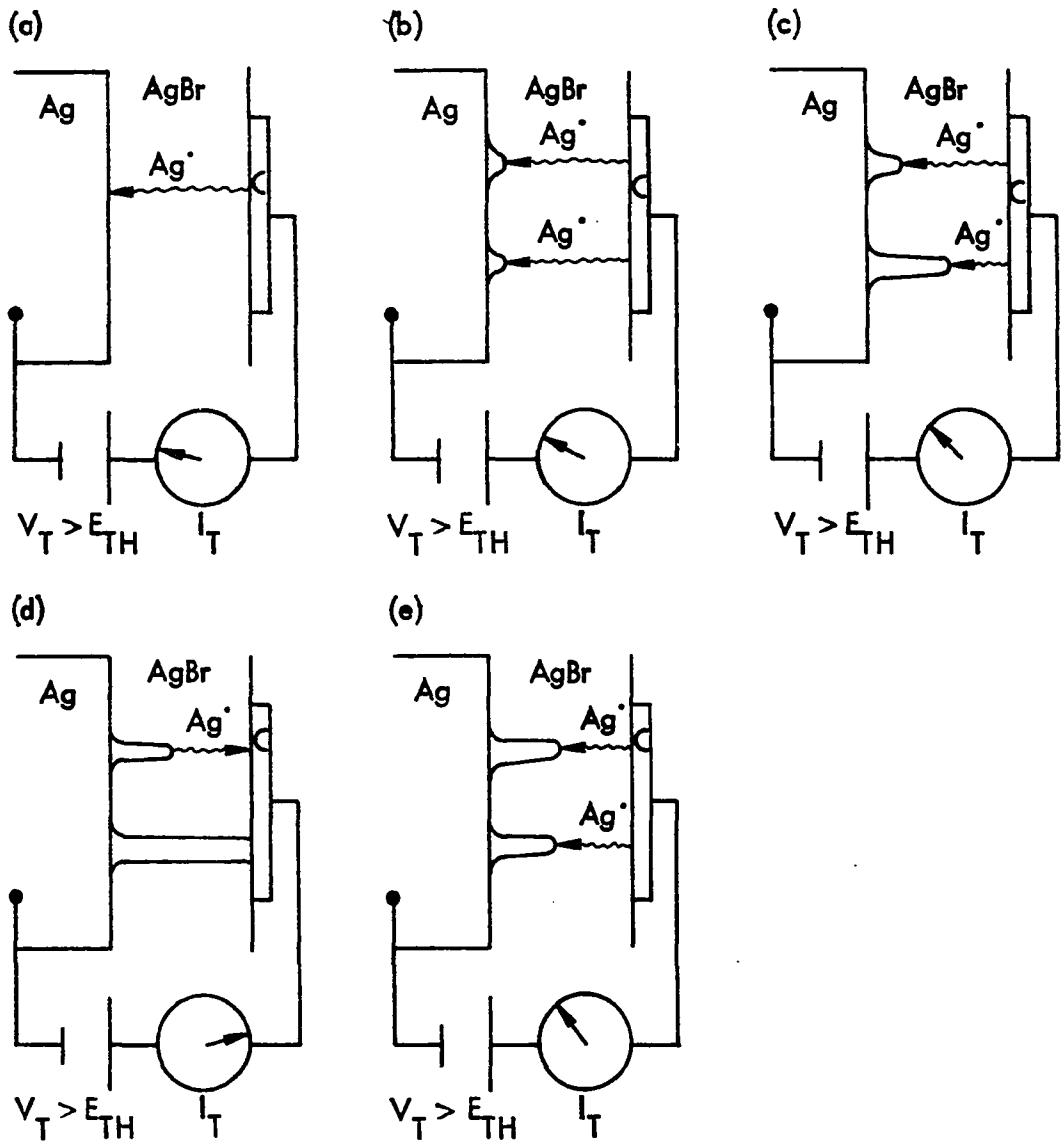

(a) Initial decomposition of AgBr at AgBr, Br_2 interface
(b) Instability formation
(c) Instability growth
(d) Dendrite short circuit
(e) Dendrite annihilation with subsequent growth

Figure 8. Proposed sequence for electrolysis induced dendrite formation in AgBr scaling layers. $V_T > E_{TH}$.

an induction furnace. Observation of the silver interface with both optical and scanning electron microscopes revealed that a large number of silver dendrites had been formed and retained. Figure 9 shows photomicrographs of these dendrites in several different specimens at various magnifications.

The behavior just described was observed in two constant voltage experiments in which 1.0 volt and 5.0 volts were applied to the cell; and in two constant current experiments in which 30 and 40 mA were applied cathodic to silver. In the constant current experiments dips or abrupt minima in the measured voltages were observed with time. Dendrite formation in AgBr similar to that observed here was found by Tubandt (48) in his classical transference number measurements on silver and cuprous halides. In his experiments AgBr pellets were sandwiched between two silver electrodes. Because Tubandt had no source of bromine with which to annihilate the silver dendrites, his cells remained short circuited after the first dendrite reached the anode. Thus, the results of this work and the earlier work of Tubandt show that planar decomposition of AgBr scales is not possible when silver electrodes are used. Instead instabilities form at the silver, silver bromide interface which grow and short circuit the cell.

Generalizations concerning this effect on other scaling systems based solely on the diffusional arguments presented above cannot be made, however, since surface and strain energy considerations could be important. For example, Tubandt (48) failed to observe dendrite formation in his transference number measurements on silver iodide even though silver iodide, like silver bromide, conducts electricity

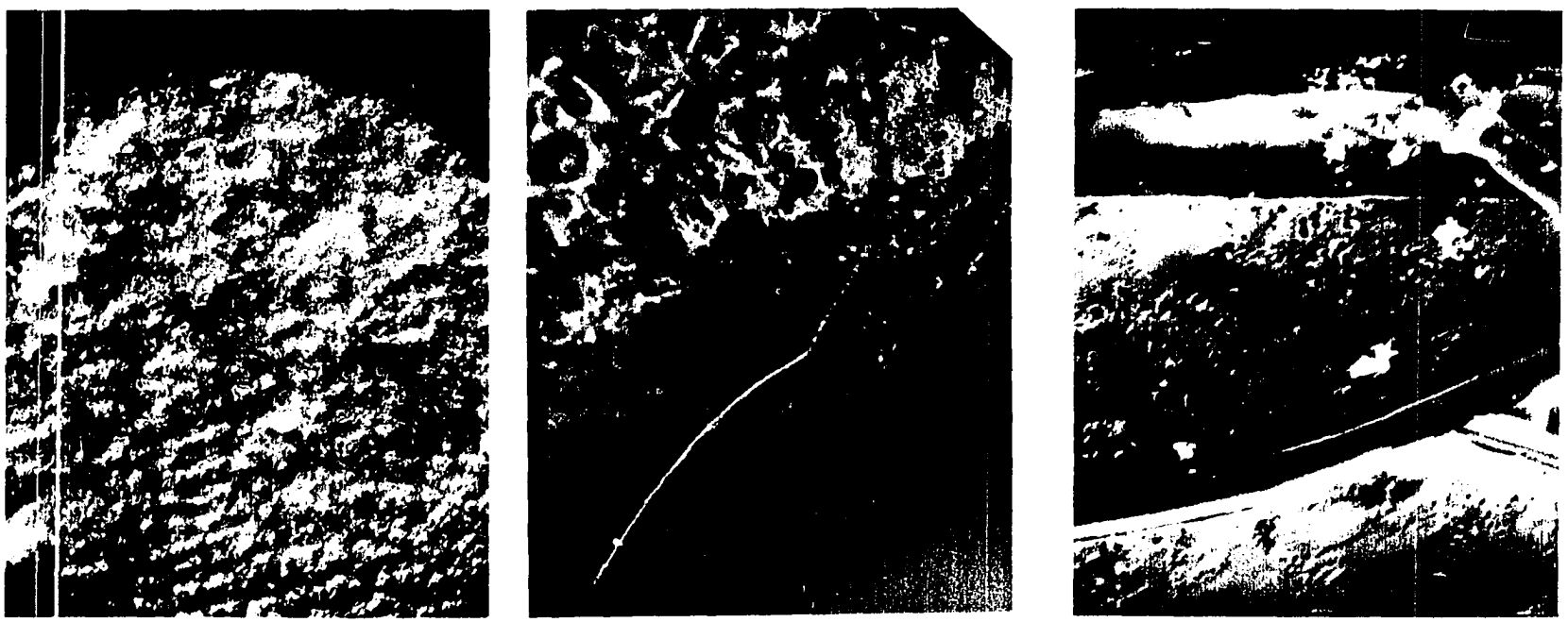

(a) (b) (c)

Figure 9. Photomicrographs of the silver dendrites formed in the decomposition experiments. a) Optical micrograph of the silver dendrites (X 90). b) Optical micrograph of a single silver dendrite (X 97.5). c) SEM micrograph of several silver dendrites (X 750).

by silver ion migration. It is apparent that other considerations in addition to diffusional arguments come into play in explaining why this phenomenon is absent in AgI.

Accelerated bromination experiments A number of experiments were run in order to accelerate the bromination rate of silver under potentiostatic conditions. Again, special effects were encountered which eventually violated the planar geometry assumptions of the theory. These effects were manifested as currents that were much smaller and which decayed much more rapidly than the theoretical calculations predicted. The calculations were based on known conductivity data for AgBr. Thus, experimental plots of I_T^{-2} versus $t - t_0$ were not strictly linear as predicted and, moreover, exhibited excessively large slopes and intercepts.

Again, the experimental cells were examined to diagnose the origin of the above departures. In each cell it was found that the AgBr scale had grown around the walls of the graphite electrode presumably according to the mechanism outlined in the sequence in Figure 10. In Figure 10a the cell is at open circuit, and the bromine can penetrate into the AgBr, C interface to consume silver ions as fast as they arrive to form AgBr. As soon as the potential is applied, an enhanced migration of silver ions is exhibited so that now bromine cannot penetrate the AgBr, C interface rapidly enough to meet the extra demand. The silver ions then migrate to the periphery of the graphite electrode where bromine is more plentiful as shown in Figure 10b. The AgBr which forms at the edge of the graphite electrode then seals the AgBr, C interface from further bromine penetration as

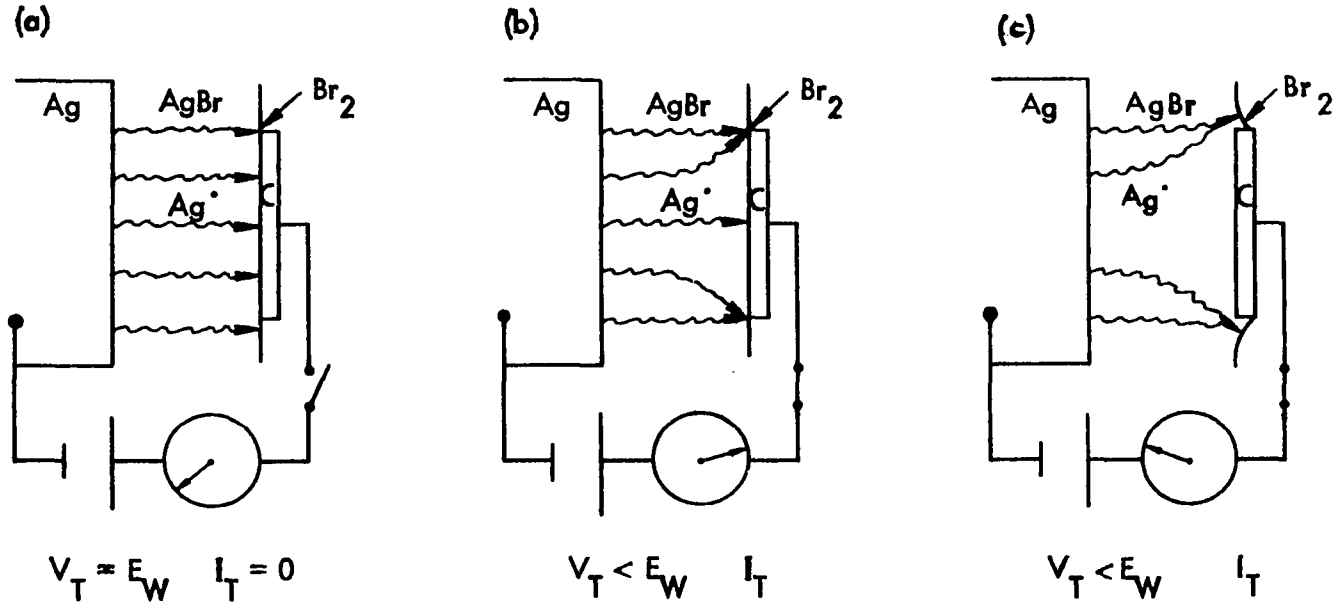

Figure 10. Proposed sequence for local cell action at the anode periphery during accelerated bromination experiments. $V_T < E_W$.

shown in Figure 10c. Thus, the amount of current which can flow is limited by the rate at which silver can diffuse to the edge of the graphite electrode where the three phases are in contact; namely, graphite, AgBr and Br_2. Experiments of this type were run in which applied voltages ranged from $0 < V_T < E_W$. Currents were lower and decayed much more rapidly than would be predicted from the theoretical formulas presented above.

Thus, dendrite formation occurred in the voltage range, $V_T > E_{TH}$, and localized cell action at the anode periphery occurred in the voltage range $V_T < E_W$. Both of these effects altered the geometry of transport kinetics (i.e., the planar assumption was violated) in the scale so drastically as to preclude a direct comparison of the kinetic formulas derived in the theoretical section and in Appendix B with the experimental results. Nevertheless, the observed behavior can be rationalized qualitatively if the geometrical alterations are taken into account.

Silicon Oxidation

Unlike AgBr, little is known about the intrinsic mechanisms of electrical conduction in SiO_2 (17, 18). Whereas trace amounts of impurities produce negligible increases in the total conductivity of AgBr, trace impurities such as aluminum-, alkali-, hydroxyl- and hydrogen ions produce increases of several orders of magnitude in the total conductivity of SiO_2 (see, for example, references 17, 18, 49). This is because intrinsic SiO_2 is nearly an insulator even at 1000 °C.

Thus, relatively few attempts have been made to measure the conductivity of undoped or intrinsic SiO_2. In the few studies that have been made a large amount of disagreement exists in the conductivity data reported by different investigators partly because the specimens of "pure" vitreous silica were obtained from different sources.

As techniques have improved the purity of silica, the reported conductivity has decreased. The lowest conductivities to date have been reported by Jorgensen and Norton (50) for Corning 7940 fused (amorphous) silica and by Laverty and Ryan (5) for thin amorphous SiO_2 films. The measurement of Jorgensen and Norton was made on an oxygen permeability cell with 6 Torr of oxygen on the high pressure (P''_{O_2}) side and 10^{-7} Torr total pressure on the mass spectrometer side of the cell. Their reported conductivity value of 2.2×10^{-9} $ohm^{-1}cm^{-1}$ at 1000 °C, therefore, amounts to a spatial average through the SiO_2 film. This value is very difficult to interpret quantitatively, however, because among other things, the oxygen pressure on the mass spectrometer side of the cell is probably highly uncertain.

Laverty and Ryan (5) measured the total conductivity of a thin film of SiO_2 on a silicon substrate at 850 °C. Their cell design was of the type $O_2|Pt|SiO_2|Si|SiO_2|Pt|O_2$ so that a P_{O_2} or μ_{O_2} difference existed across each of the SiO_2 layers in the cell. Thus, their value of 5.3×10^{-11} $ohm^{-1}cm^{-1}$ at 850 °C also corresponds to a spatial average over the μ_{O_2} profile set up in the SiO_2 layers. However, at least the oxygen chemical potential was well defined at both electrodes. Nevertheless, their average value is still not amenable

to quantitative interpretation unless hypotheses are introduced regarding the defect structure and μ_{O_2} profiles to be expected in SiO_2.

In contrast to these conductivity studies, measurements of the scaling rate constant of silicon and oxygen permeability in SiO_2 have been more successful. These measurements can be easily correlated (51), and good agreement is found. The scaling rate constant (5, 30), oxygen permeability (28) and diffusivity (29) have been observed to obey a linear oxygen pressure dependence suggestive of neutral transport in SiO_2. However, measurements were only made over one order of magnitude in P_{O_2}.

It is necessary to know the mechanism of mass and charge transport (defect structure) in SiO_2 in order to obtain detailed predictions of the kinetics of SiO_2 film thickening and thinning under potentiostatic and galvanostatic conditions. This is because predicted rates may vary considerably with transport mechanism. The two general transport models to be considered here are the constant ionic conductivity model and the constant ionic transference number model. Apparently SiO_2 is neither a predominant ionic or electronic conductor (3); hence, it is not certain a priori which is the correct mechanism.

The constant σ_{ion} model assumes that predominant ionic conduction exists in the mixed conductor over a significant range of P_{X_2}. This assumption requires that nearly equal concentrations of vacancies and interstitials exist in the material (52) as is the case, for example, in AgBr. Revez (53) has pointed out that vacancy migration in SiO_2 is energetically unfavorable due to the rigidity of the silicon-oxygen tetrahedra comprising the SiO_2 network. The term

network is used here instead of lattice because SiO_2 films are amorphous in nature. Instead it is much easier for oxygen ion interstitials to migrate through the SiO_2 network with charge compensation due to hole migration (53). This latter conduction scheme is consistent with the constant t_{ion} model. Nevertheless, both models have been examined for SiO_2, and predictions for the thickening and thinning kinetics are delineated and discussed below.

A number of independent measurements can be made to infer the transport mechanisms in a mixed conducting scale compound. Two of the most reliable methods are to measure the open circuit emf, E_W, and the total electrical conductivity, σ_T, of the compound as functions of temperature and partial pressure or chemical potential of the nonmetal species (52, 54). Measurements of the scaling rate constant of a metal as a function of partial pressure and temperature can also yield useful results (54). Frequently the nonmetal chemical potentials are fixed with the use of coexistence electrodes (52) although gas phase equilibria, for example, H_2/H_2O and CO/CO_2 mixtures in conjunction with porous platinum electrodes have also been used (52). By employing these types of reversible electrodes, E_W and σ_T can be measured over many orders of magnitude in P_{X_2}.

Unfortunately coexistence electrodes must not be used in conjunction with SiO_2 if one is to prevent diffusional contamination of the SiO_2 by the electrode metal. Such contamination would certainly swamp the intrinsic defect nature of SiO_2 thereby undermining the validity of emf and conductivity measurements. Since many gaseous constituents also diffuse into SiO_2, the use of gas phase equilibria

such as H_2/H_2O and perhaps CO/CO_2 could be expected to also alter the intrinsic nature of SiO_2 again producing dubious results. Thus, the only conductivity studies that have been reported to date for pure SiO_2 have involved pure oxygen gas or oxygen plus inert gas mixtures together with porous platinum electrodes which presumably do not contaminate the SiO_2. Some of these studies (5) have involved non-symmetric conductivity cells with the SiO_2 grown on pure silicon immersed in oxygen gas. Thus, the endpoint P_{O_2} values are P''_{O_2} = 1 atm and $P'_{O_2} = P^{eq}_{O_2}$ given by Si, SiO_2 coexistence. Similarly, a few open circuit emf measurements have been made across such cells (3).

Open circuit emf measurements

A large number of open circuit emf measurements were made on non-symmetric cells of the type $Si|SiO_2|Pt|O_2$ in order to determine the average ionic transference number of SiO_2. Most of these measurements were made on cells with initial film thicknesses of 1500 to 2000 Å. These measurements were carried out as preliminary studies in each of the applied electric field experiments. Although a scatter of $\pm$ 50 mV was observed for all of the experiments, most of the observed emf values were in the vicinity of 420 mV. This corresponds to an average ionic transference number of 0.24. Other values for the average ionic transference number have been reported in the literature ranging from 0.40 to 1.0 (3, 50, 55) depending on the purity of the SiO_2; however, the value of 0.24 was used for the theoretical calculations in the present work.

Scaling rate measurements

The scaling kinetics of silicon were measured at 850 °C in order to make an independent determination of the scaling rate constant of silicon to be used in subsequent calculations. The procedure was to oxidize a silicon specimen for a known length of time, etch off part of the SiO_2 with a buffered HF solution and then determine the oxide thickness with the use of optical interferometry. This technique is convenient and inexpensive; however, accuracy is only to within 10% for thicknesses from 1000 to 5000 Å (56).

The data are presented in Figure 10 and are compared with the results of Jorgensen (3) and Deal and Grove (30) for the oxidation of pure and heavily doped silicon, respectively. Because of the differences in scaling kinetics observed by these investigators, several experiments were run. It can be seen from the figure that the data obtained in the present study are in close agreement with the results of Jorgensen. The slope of the L^2 versus time plot yields a scaling rate constant of 1.25×10^{-11} cm^2/h at 850 °C.

It will be shown below that neutral transport in SiO_2 is negligible. Thus, the value for the scaling rate constant obtained here will be interpreted to be that due solely to oxygen ion migration. This value for $k + k_n \approx k$ is used in conjunction with the value for E_W reported in this work to deduce conductivity parameters necessary for predicting the effect of applied electric fields on silicon oxidation for both the constant t_{ion} model and the constant σ_{ion} model. The derivations are presented in Appendix D and Fortran computer

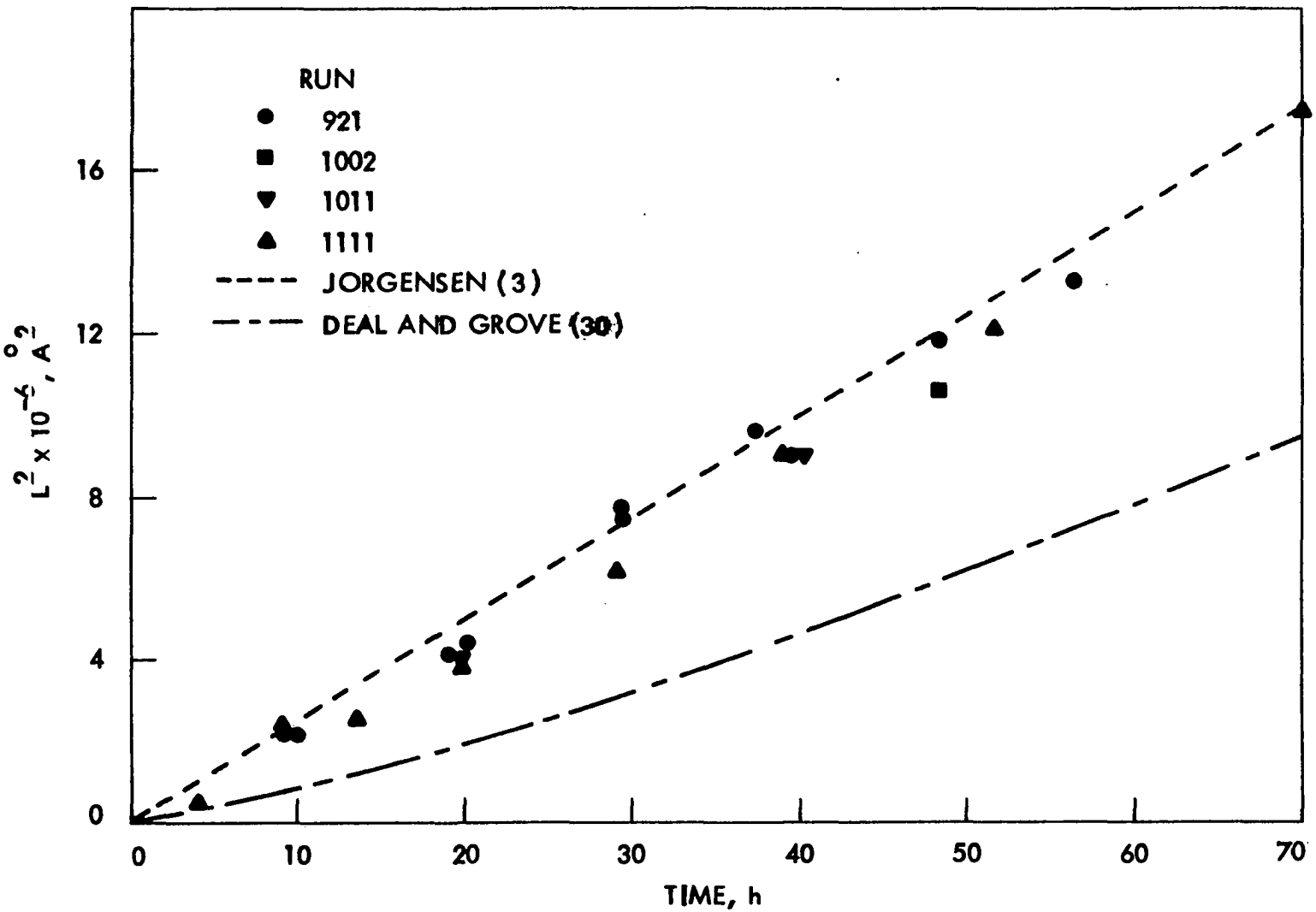

Figure 11. Measurements of the scaling rate of silicon in pure oxygen at 850 °C under open circuit conditions.

programs calculating the galvanostatic scale thickening and thinning kinetics for SiO_2 films are given in Appendices F and G.

Applied electric field experiments

Potentiostatic scaling kinetics Most of the applied electric field experiments were run under constant voltage; i.e., potentiostatic conditions. This is because the current-time data can be simply converted to plots of I_T^{-2} versus $t - t_0$ which should be linear as was pointed out in the theoretical section. Also according to the theory such linearization of the data is not possible for the galvanostatic case.

The experimental procedure was to heat the preoxidized silicon cell assembly containing the platinum electrodes and lead wires in vacuum to 850 °C. Oxygen was admitted into the system, and the open circuit emf was monitored until a steady state value was obtained. Constant voltages ranging from 0.0 to 5.0 volts were then applied to the cell using the operational amplifier scheme shown in Figure 6a. Accelerated growth should be exhibited in the voltage range $0.0 < V_T < E_W$ and retarded growth in the voltage range $E_W < V_T < V_{Halt}$ where $E_W = 0.42$ volts. In the voltage range $V_T > V_{Halt}$, decomposition should be exhibited. If the flux of neutral oxygen is negligible in SiO_2, V_{Halt} will be the thermodynamic emf. The thermodynamic emf has been calculated from thermochemical data (57) and is 1.754 volts at 850 °C. Due to the symmetric nature of the cells, only half of the cell was used for the applied electric field experiments as shown

in Figure 12. The open circuit emf and conductance were measured across the other half of the cell.

Platinum and silicon form a eutectic at 830 °C (58) so that loss of the center lead by eutectic melting most generally limited the life of the cell. Care was taken during the cell fabrication to guard against tension in the center lead, and observing this precaution greatly extended cell life. However, after prolonged exposures to oxygen, on the order of weeks, oxide formation eventually separated the center platinum lead from the silicon substrate and terminated the useful life of the cell.

Decomposition experiments Voltages in the range $1.80 < V_T < 5.00$ volts (cathodic to silicon) were applied over SiO_2 films thermally grown to thicknesses of 5000 Å on silicon. Jorgensen's galvanostatic thinning experiments (4) showed that electrolytic decomposition of SiO_2 films proceeds uniformly thus preserving their planar geometry. It was, therefore, anticipated that potentiostatic decomposition would likewise preserve the planar scale geometry during thinning and would give rise to the timewise current increases predicted in the theoretical section.

In the present investigation, however, localized breakdown of the SiO_2 films occurred as evidenced by highly sporadic current fluctuations. Moreover, this phenomenon was observed in all experiments where voltages greater than 1.8 volts were applied. This fact seems to be totally inconsistent with Jorgensen's experiments because his voltages decayed through precisely the same range of values during galvanostatic decomposition and yet the films reportedly did not fail locally. In

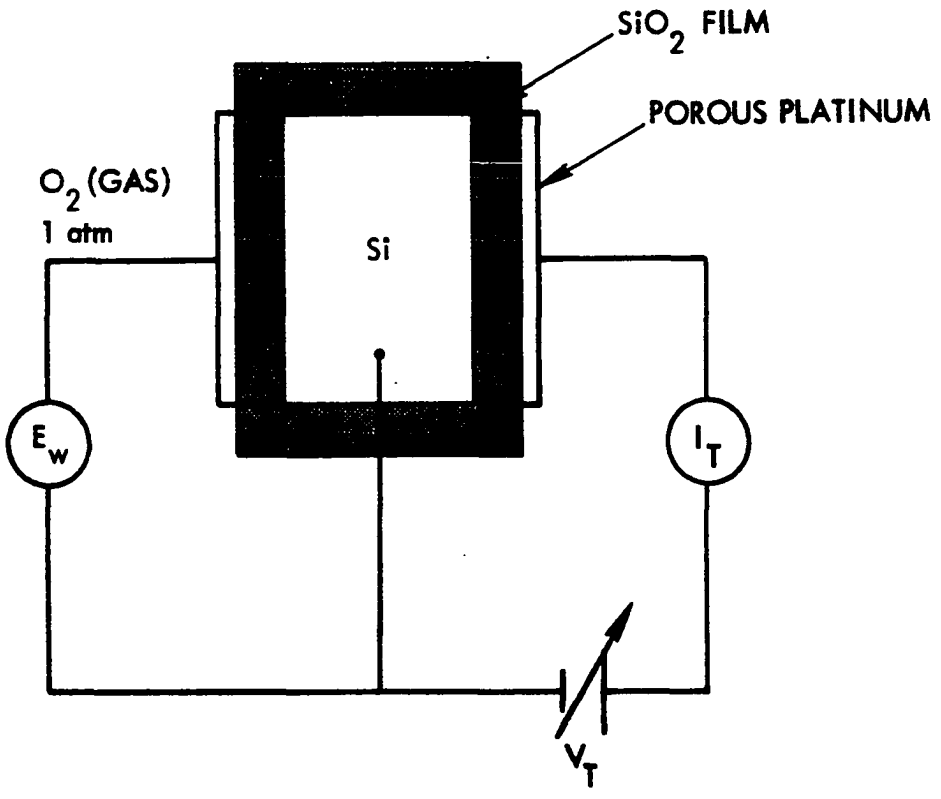

Figure 12. Schematic diagram of the cell arrangement and external electrical circuitry used to study the kinetics of SiO_2 scale thickening and thinning. Constant voltages and currents were applied with the circuitry shown in Figure 6.

retrospect, it is tempting to speculate that the platinum to silicon contact (see Figure 12) in Jorgensen's experiments had been separated by SiO_2 formation, thus shifting a significant but unknown portion of the voltage drop off the SiO_2 layer that was being thinned. If this is so, one must interpret Jorgensen's findings in terms of a double cell involving not one but two layers of SiO_2. Raleigh (14, 16) has also suggested this possibility in attempting to rationalize Jorgensen's results as will be discussed later. Such an interpretation would be greatly complicated by geometrical considerations among other things and would also require knowing the voltage over both SiO_2 scales individually. Hence, no further speculation on this matter is offered. In the present investigation, however, the unanticipated localized breakdown behavior precluded a quantitative interpretation of the voltage versus time data in the decomposition mode. However, a description of these observed effects and a qualitative interpretation will be given.

Figure 13 shows the planar surface of a typical specimen after exposure to a potentiostatic decomposition experiment at 850 °C. In Figure 13a the specimen had been prepared by first etching the platinum electrode away in aqua regia and then removing most of the SiO_2 with HF. This leaves the silicon substrate surface only partially exposed while the remainder is still covered with adherent flakes of SiO_2 scale. It is evident from Figure 13a that localized pits have been excavated in the silicon substrate, some have penetrated through the SiO_2 flakes and finally some appear to be forming beneath undamaged regions of these flakes. Figure 13b merely shows the same specimen

(a)

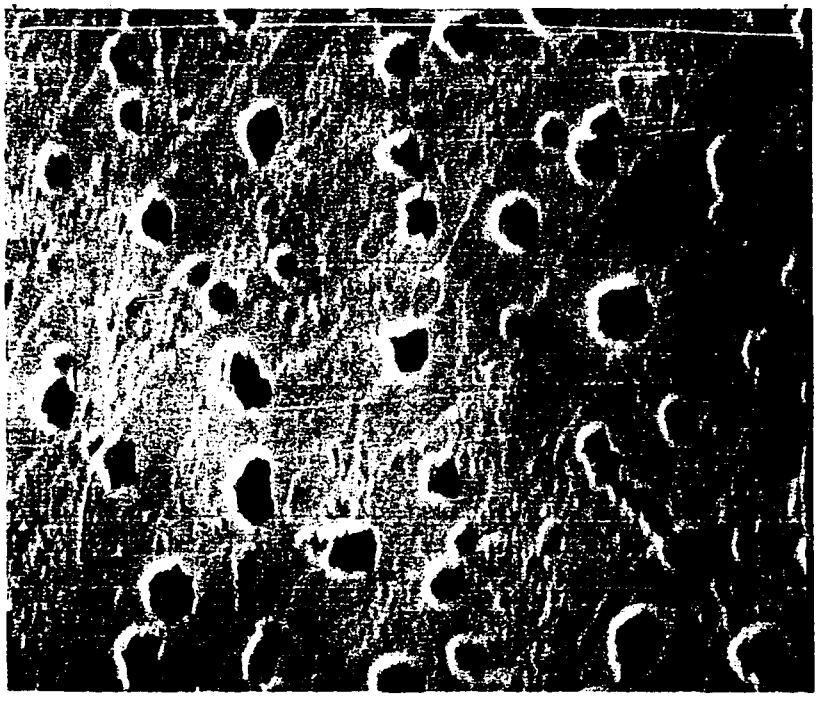

(b)

Figure 13. SEM micrographs of damage to the Si, SiO_2 interface in a decomposition experiment. a) Partially etched specimens showing breakdown damage pits in the silicon substrate surface and in the retained flakes of SiO_2 (X 3000). b) Pits in the silicon substrate of a fully etched specimen (X 3000).

(different region) after complete removal of the SiO_2 with the HF etchant. Features of these types were observed for all decomposition voltages greater than 1.8 volts, and the following explanation in terms of localized electrolytic decomposition followed by catastrophic dielectric breakdown is offered.

According to Klein (59) catastrophic dielectric breakdown occurs in three stages. In the initial stage a localized avalanche of carriers is initiated when the local voltage gradient exceeds some critical value typically in the range of 10^5 to 10^7 V/cm for insulators. Snow and Deal (60) found this critical value to be 8×10^6 V/cm for SiO_2 films at room temperature. Localized I^2R type heating results which causes the current to run away during the second phase of breakdown because the conductivity of insulator materials increases exponentially with temperature. In the final stage current arcing vaporizes the electrode materials as well as the interposed dielectric insulator in the immediate vicinity of the arc. The damaged region then becomes a nonconductive void, and the breakdown is said to be self healing (59).

In addition to dielectric breakdown, electrolytic breakdown can also occur if mobile ions prevail in the compound. A most important difference between these two modes of breakdown is that electrolytic breakdown is induced by a critical voltage difference (namely, the thermodynamic emf if $J_{X_2} = 0$) but is otherwise independent of the voltage gradient in the specimen. Dielectric breakdown, on the other hand, commences only after a critical voltage gradient is surpassed but is otherwise independent of total applied voltage. In view of

these concepts the observed breakdown effects can be rationalized with the aid of the sequence shown in Figure 14.

In the initial stage, shown in Figure 14a, electrolysis of SiO_2 commences at the Si, SiO_2 interface. Suppose that small protuberances form as highly conductive, partially reduced pockets of SiO_2 (Figure 14b). Then, once formed, the tip of the most protruding SiO_2 pocket propagates ahead of the others and ahead of the planar interface. That is, the oxygen removal rate from the tip of this protuberance is greater than that from all the other points. This is because the average field gradient from that tip to the anode is greater than that between all the other cathode locations and the anode. Thus, the pocket of partially reduced SiO_2 evolves into a dendritic spike in a runaway mode of propagation.

As the tip of the reduced SiO_2 dendrite gets closer to the anode, the local voltage gradient in front of it continues to increase even though the applied voltage remains constant. Eventually the critical gradient (about 8×10^6 V/cm) required for the catastrophic dielectric breakdown of SiO_2 is exceeded whereupon arcing vaporizes the remaining path length as shown schematically in Figure 14c. In this way the short circuit is broken, and the breakdown is self healing. Thus, the whole process starts over again at the next largest conductive protuberance on the cathode.

The electrolytic breakdown phenomenon observed here provides strong evidence for the domination of charged over uncharged oxygen migration in SiO_2. Significant migration of neutral oxygen would tend to annihilate the protuberances as they approached the anode.

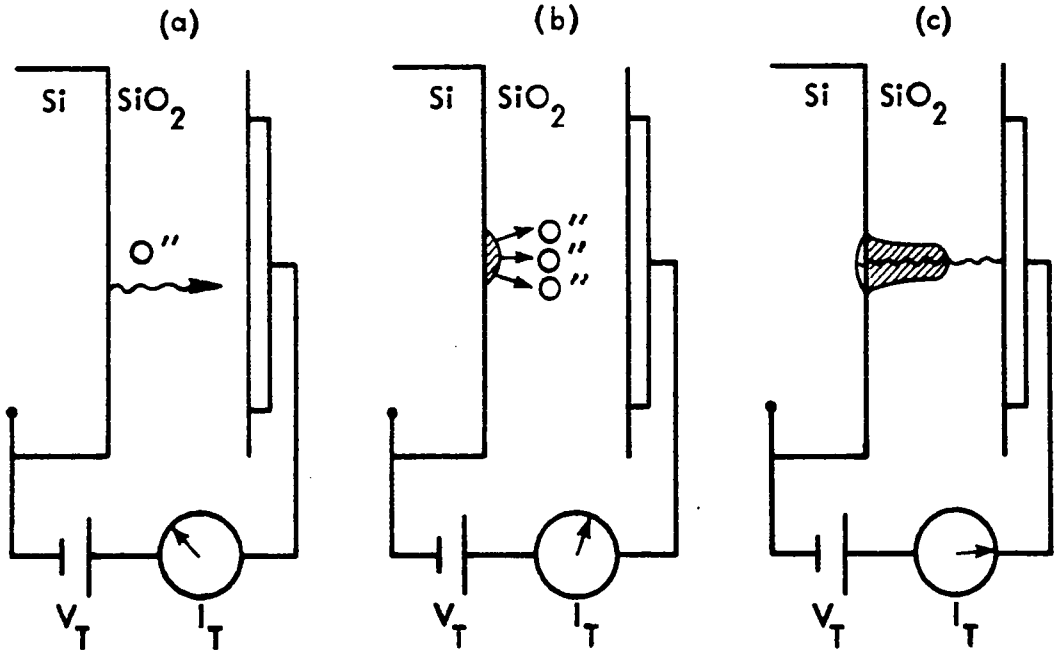

(a) - Initial decomposition of Si, SiO_2 interface

(b) - Formation of region of highly reduced SiO_2

(c) - Growth of reduced region with subsequent arcing due to dielectric breakdown

Figure 14. Proposed sequence for electrolysis induced dielectric breakdown for SiO_2 layers at elevated temperatures.

Furthermore this phenomenon occurred at all voltages greater than the thermodynamic emf. In view of Eq. [20] this implies that J_{O_2} is negligible. Were the flux of neutral oxygen nonzero, a voltage considerably greater than E_{TH} would have had to be applied to cause electrolytic breakdown. Finally the fact that these protuberances grow from the cathode instead of the anode requires that oxygen ions as opposed to silicon ions carry the electrolysis current. Evidence for this has also been reported previously by Jorgensen (3) and Karube et al. (61).

To further substantiate the foregoing mechanism of electrolysis induced breakdown, similar studies were conducted with applied voltages of opposite polarity. Such voltages would not be expected to give rise to pockets of electrolytically reduced SiO_2 because the pockets would now have to form at the platinum electrode where the abundance of oxygen gas would immediately reoxidize them. Such reoxidation would reconvert the pockets to insulators thus arresting the electrolysis current required for the breakaway propagation mode. Hence, catastrophic breakdown with reverse bias should require much larger applied voltages because now the critical gradient of $\sim 8 \times 10^6$ V/cm must be set up over the entire thickness of the SiO_2 film. For an initial thickness of 5000 Å the required voltage would be about 400 volts at room temperature. The experiments revealed no breakdown below 120 volts with catastrophic breakdown above that value. The observed voltage is sufficiently close to the predicted value to serve as a confirmation. The critical voltage gradient at elevated temperatures has not been previously measured; however, one would expect this gradient to be

somewhat less than the room temperature value of 8×10^6 V/cm given by Snow and Deal (60).

The cell used for this study was observed under the scanning electron microscope with the platinum electrode still intact. SEM micrographs of the breakdown pits are shown in Figure 15. In the lower SEM micrograph breakdown was probably assisted by, or perhaps caused, a crack in either the silicon substrate or the SiO_2. The pits which formed with reverse polarity are much larger than those shown in Figure 13 which is an indication of the additional energy input necessary to cause the breakdown.

Accelerated and retarded oxidation experiments Constant voltages ranging from 0.0 to 1.75 volts were applied cathodic to silicon in order to accelerate or retard the scaling rate. A gentle current decrease with time was expected due to scale thickening; however in each experiment, an excessively rapid current decay was observed with current magnitudes being much smaller than anticipated. Moreover, data plots of I_T^{-2} versus $t - t_0$ exhibited nonlinearity for all of the experiments which suggests electrode nonreversibility.

This suspicion was apparently born out by an experiment in which the voltage was increased at intervals while the steady state current was measured. Virtually linear plots of I_T versus V_T would indicate truly reversible electrode behavior; however, a nonlinear plot with downward curvature was obtained. Nonlinear plots of this type suggest that at least one of the electrodes was suffering a degree of polarization.

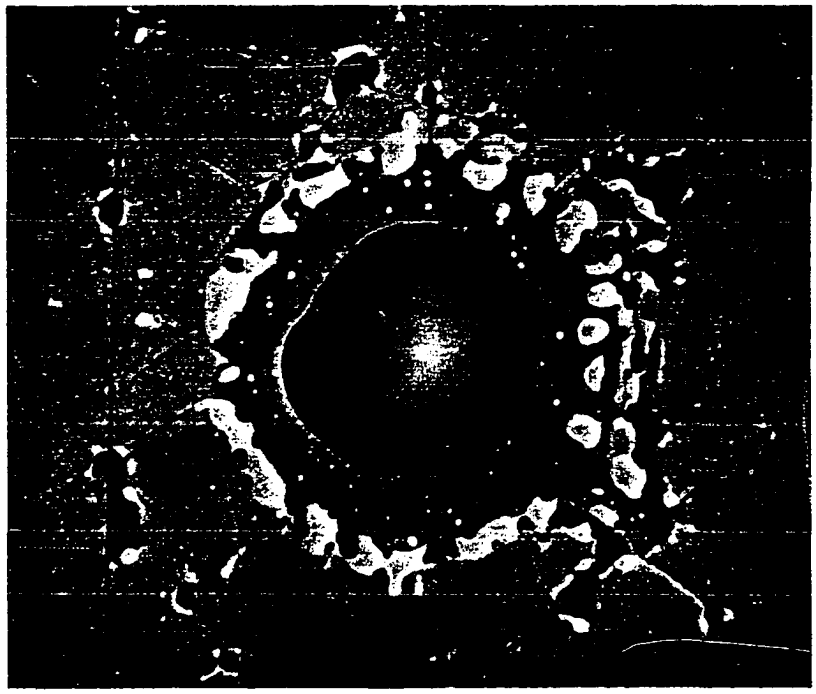

(a)

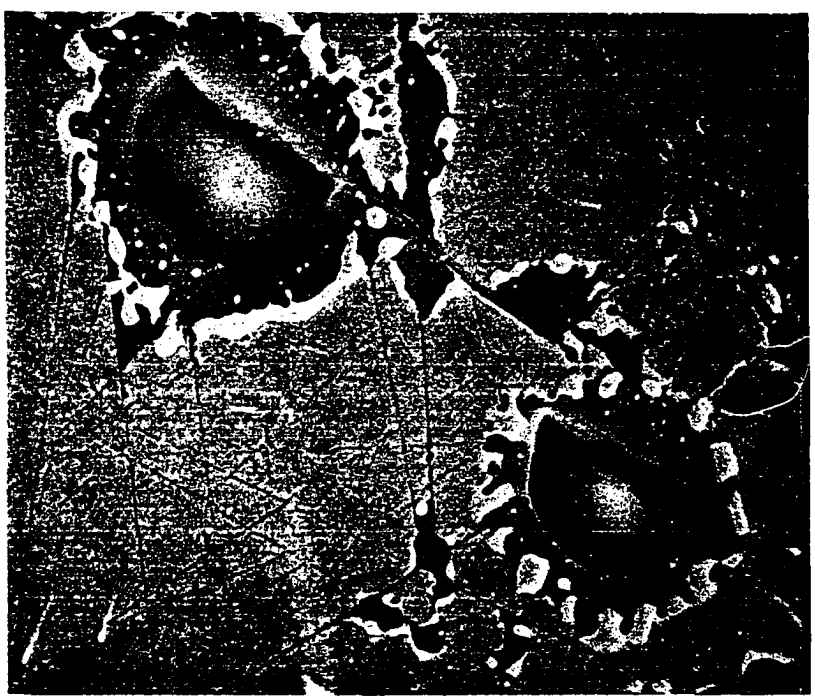

(b)

Figure 15. SEM micrographs of self healing electrical breakdown of a SiO_2 film induced by a large accelerating field. a) Breakdown in a defect free region of the SiO_2 film (X 1500). b) Breakdown along an imperfection (X 1500).

The two different types of platinum electrodes described earlier were tried in an attempt to improve electrode reversibility. The sputtered platinum electrodes obtained from NASA Lewis Research Center apparently volatilized and were lost after a few hours at 850 °C. The electron beam evaporated electrodes lasted the duration of the experiments; however, the same polarization effects were exhibited by all of the electron beam evaporated electrodes despite the fact that they were provided from two independent sources. Further attempts to improve electrode performance were abandoned primarily because of inaccessibility to a suitable sputtering facility.

Galvanostatic scaling kinetics Several applied electric field experiments were conducted under constant current; i.e., galvanostatic conditions. Again, electrode polarization effects were encountered as evidenced in this case by excessively rapid voltage transients. A typical V_T versus time plot for these experiments is shown in Figure 16. The constant current of 1μA was applied cathodic to silicon with the intention of retarding scale growth. The initial voltage increase shown in the figure is too rapid to be interpreted in terms of oxide scale thickening.

Thus, the experiments carried out as part of the present work could not be used to quantitatively confirm the applicability of the theoretical formulas developed in the theoretical section and the appendices. It has been argued, however, that this was due mainly to cathodic polarization and related geometrical effects which could not be circumvented with the electrode fabrication facilities available.

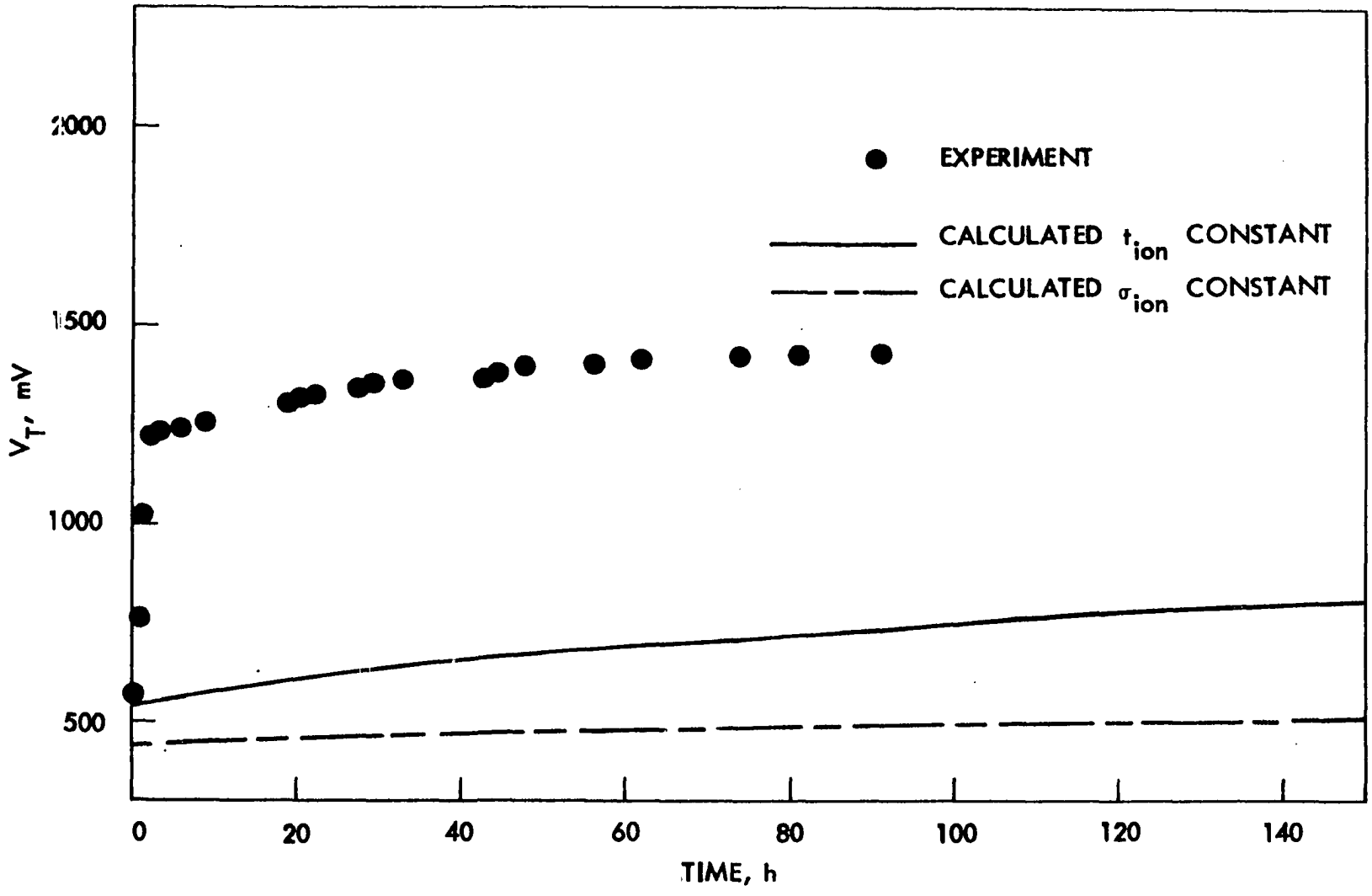

Figure 16. Plot of V_T versus time for a typical galvanostatic retarded oxidation experiment at 850 °C. I_T = 1μA cathodic to silicon; L_0 = 1750 Å.

It is, therefore, of interest to examine the earlier results of Jorgensen (3, 4) in the light of the same formulas to see if acceptable agreement is realized for those experiments This is especially interesting not only because Jorgensen took special care to develop a sputtering procedure which he states provides a reversible porous platinum electrode on the SiO_2 surface, but also because he reported no electrolytic or dielectric breakdown effects during SiO_2 decomposition. Indeed he reports that thermally grown SiO_2 films decompose uniformly thus preserving the planar scale geometry assumed in the theoretical development.

Comparison of theory to previous galvanostatic studies

Jorgensen studied the galvanostatic scaling kinetics of silicon of 850 ^{o}C under conditions of accelerated growth (3), retarded growth (3) and decomposition (4) in which plots of V_T versus time were presented. The case of accelerated growth can only be discussed qualitatively because Jorgensen did not report the initial film thickness L_0 nor the constant applied current I_T that was used. Nevertheless, it can be said that the linear plots of V_T^2 versus time obtained by Jorgensen do not seem to be in qualitative accord with the theoretical predictions of the present theory. In particular, it was shown in the theoretical section that parabolic scaling kinetics, as revealed by linear plots of V_T^2 versus time, are not to be expected for galvanostatic experiments because the parameter r cannot be strictly independent of time. On the other hand, it might be argued that if either r or k(r, t) in Eq. [30] is a sufficiently weak function of time, then the observed parabolic dependence might be predicted at least to a first approximation.

Therefore, theoretical calculations of r and k(r) versus time were carried out for reasonable choices of L_0, I_T, the conductivity parameters of SiO_2 and their P_{O_2} dependences at 850 °C. None of these choices; however gave an acceptable fit to Jorgensen's plots. Further attempts to determine the best fit possible were not considered worthwhile since Jorgensen had left so much of the essential information unspecified.

Jorgensen's measurements for a retarded growth experiment are compared with the theoretical predictions of the present work in Figure 17. Here the curves were calculated assuming the constant ionic transference number model with the scaling rate constant due to neutral migration, k_n set equal to zero in accordance with earlier discussion. The calculated curves for the constant ionic conductivity model fall well below the plotted curves and have been deleted for clarity. It can be seen from Figure 17 that the agreement between the theory and Jorgensen's experimental results is not striking. However, it should be mentioned here that rather important details regarding Jorgensen's experiments can be called into question. For example, Jorgensen's original data plot (3) in Figure 17 passed through the origin which contradicts the fact that V_T must be greater than E_W in order for retarded growth to occur. This is suggestive of oxide formation at the center electrode (see Figure 12). When later confronted on this point by Raleigh (14, 16) Jorgensen simply altered the plot so that in a recent paper (25), it appeared as shown in Figure 17. His rationalization for doing this goes as follows: At the beginning of the experiments, porous platinum electrodes contacted the silicon crystal in the absence of SiO_2 at 850 °C. Thus, a zero voltage

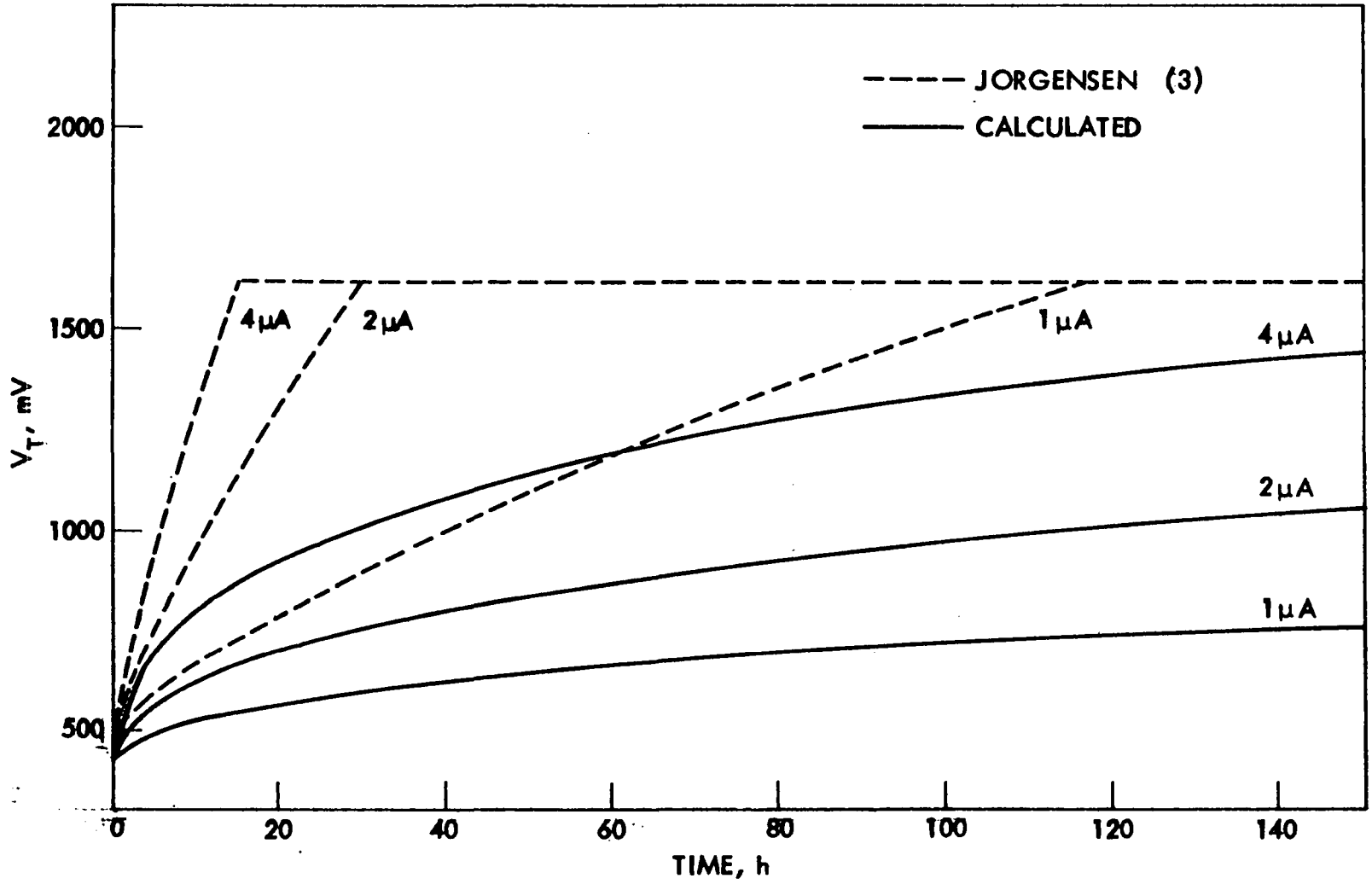

Figure 17. Comparison between theoretical predictions and Jorgensen's experimental results for galvanostatic retarded oxide growth at 850 °C. L_0 = 0 Å.[8]

reading was obtained. As soon as the oxide scale formed, the voltage was observed to jump to 0.65 volts. Thus, it was argued that the curves should have been drawn through the ordinate at 0.65 volts.

The above seems to be a gross alteration of the original data especially when several lowest V_T data points were significantly to the right of the origin. Moreover, the practicality of heating a silicon crystal to 850 ^{o}C sandwiched between two platinum electrodes in vacuum can be questioned. It is well known that platinum forms a eutectic with silicon at 830 ^{o}C (58). If the sputtered platinum electrode on the planar interface was initially in contact with the silicon (as zero initial emf values would indicate), then the eutectic reaction would be expected to permanently damage the cell. To substantiate this conjecture a silicon disk sandwiched between two platinum foil electrodes was heated in vacuum to 850 ^{o}C, exposed to oxygen and then cooled and examined. Visual as well as microscopic examination of the cell indicated that silicon had indeed attacked the platinum and that the foils had remained shorted to the silicon. Thus, no explanation for the apparent absence of this eutectic reaction in Jorgensen's experiments at 850 ^{o}C can be offered.

In a later paper Jorgensen (4) studied the galvanostatic decomposition or thinning kinetics of SiO_2 films. Shown in Figure 18 is a plot of Jorgensen's V_T versus time data compared with a theoretical calculation based on the constant t_{ion} model. The constant σ_{ion} model predicts retarded growth for the specified experimental conditions with the corresponding curve falling well below the others. It is apparent

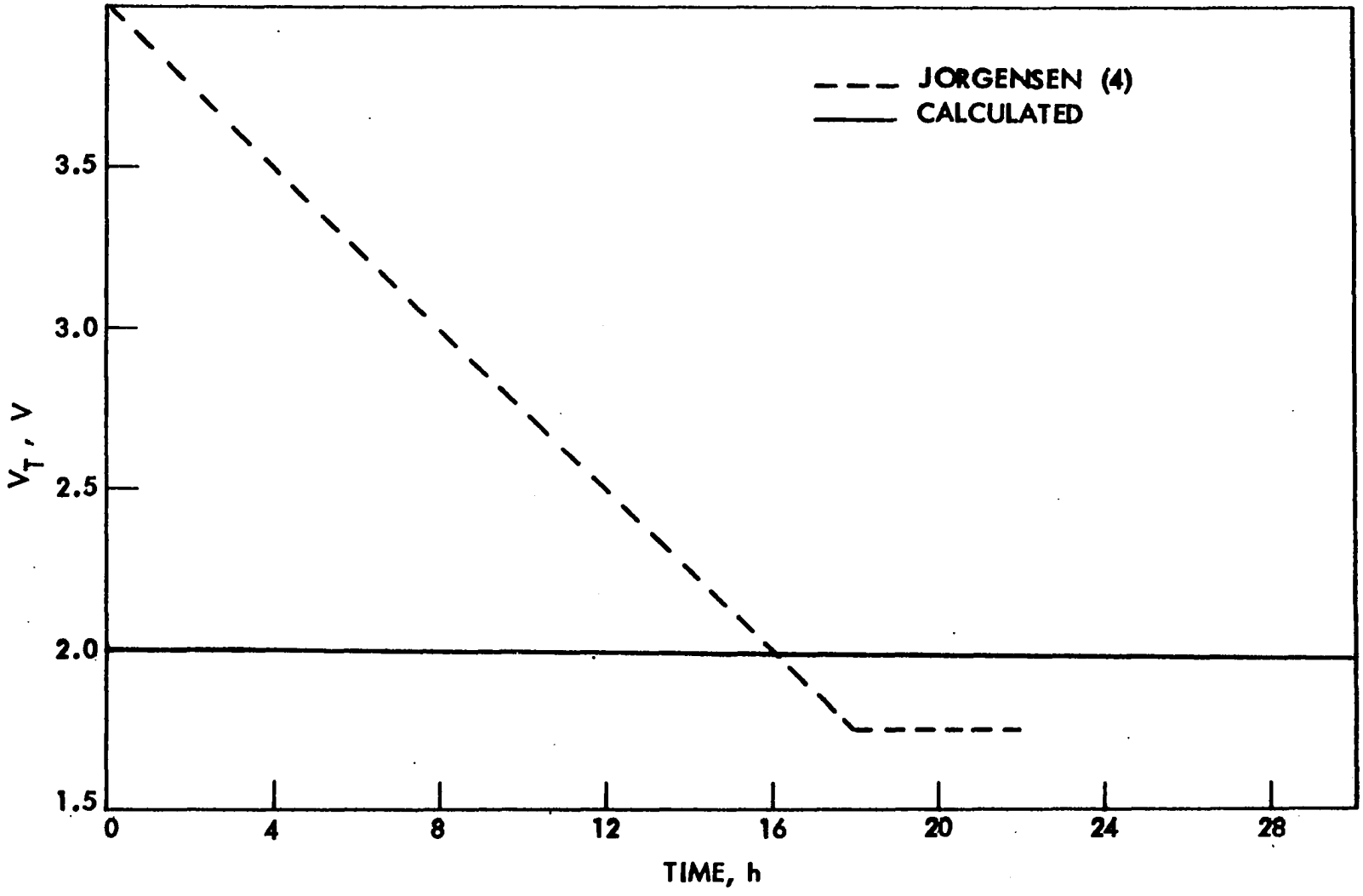

Figure 18. Comparison between theoretical predictions and Jorgensen's experimental results for galvanostatic decomposition at 850 °C. I_T = 4μA; L_0 = 5000 Å.

that a considerable disparity exists between Jorgensen's data and the theoretical predictions.

Attempts were made to force a fit between Jorgensen's data plots and the theoretical curves by arbitrarily altering the magnitudes of some of the parameters involved in the calculations; e.g., σ_T^o, t_{ion}, σ_{ion} and k_n. These alterations proved to be unsuccessful for fitting Jorgensen's data. For example, in order to approximate the slope of Jorgensen's V_T versus time plot in Figure 18, a total conductivity which is a factor of 50 less than the one used in the prediction for the constant t_{ion} model is necessary. However, this implies an intercept of 20 volts which is much larger than the 4.0 volts observed by Jorgensen. Allowing the flux due to neutral oxygen to differ from zero will increase the slope as well as the intercept; however, in view of Eq. [20] increasing J_{O_2} also increases V_{Halt} perceptibly above E_{TH} when halt voltages on the order of the thermodynamic emf were actually observed by Jorgensen. Increasing t_{ion} will improve the fit in Figure 18 but will make the fit worse in Figure 17 by increasing the intercept while V_{Halt} remains the same. Other simultaneous variations of these parameters have been tried with equally little success. Finally it is difficult to see how any theory will predict the rather abrupt corners exhibited in the plots obtained by Jorgensen unless one proposes an abrupt change in oxidation mechanism during the oxidation process. This would seem to be an unlikely possibility.

Thus, attempts to rationalize Jorgensen's data in terms of the present theory, which assumes complete diffusion control in the SiO_2 layer have been unsuccessful; notwithstanding the fact that both

Jorgensen (3, 4, 25) and Raleigh (14, 16) base their discussions qualitatively on Wagner's theory (26). Wagner's theory at open circuit (26) was extended in a logical manner in the present work, and the formulas which resulted were used to rationalize Jorgensen's experimental data. Serious disparities between the theoretical predictions and the experimental results were found. In view of the findings of this work, a theory which takes into account phase boundary reactions might be more useful. However, such a theory is beyond the intended scope of the present work which deals only with diffusion controlled scaling reactions.

SUMMARY AND CONCLUSIONS

1. A quantitative theory for the effect of applied electric fields on diffusion controlled scaling kinetics was presented. This theory predicts the kinetics of scaling layer thickening or thinning when the total current is nonzero and when a neutral flux of oxidant is permitted.

2. Definitive formulas for scale thickness, cell voltage and total current as functions of time were derived in terms of experimentally measurable quantities.

3. A quantitative formula was derived which predicts the voltage necessary to arrest scale thickening or thinning. This voltage must exceed the thermodynamic emf by a well defined amount proportional to the flux of the neutral oxidant species. When no neutral transport is possible, the halt voltage converges to the thermodynamic emf.

4. The formulas developed in this work were used to show that the theory (which is basically Wagner's theory extended to applied field conditions) does not constitute an adequate description of the effect of applied fields on the oxidation of silicon in dry oxygen. This is contrary to claims, based on qualitative arguments, previously made in the literature.

5. It was shown experimentally that applying voltages greater than the thermodynamic emf (the substrate being the cathode), to the scaling systems Ag, AgBr and Si, SiO_2 renders the initially planar scale geometries unstable. Invariably highly localized reactions take place in the decomposition mode as manifested by silver dendrite

formation in the AgBr layers and by electrolysis induced dielectric breakdown in the SiO_2 scaling layers.

6. From the breakdown voltages and morphologies for the SiO_2 films, it may be concluded: (A) that oxygen ions as opposed to silicon ions are responsible for electrolysis currents in SiO_2; and (B) that neutral oxygen fluxes in SiO_2 are negligible in comparison to the current carried by the oxygen ions.

REFERENCES

1. H. H. Uhlig and A. E. Brenner, Acta Met., 3, 108 (1955).

2. D. Cismaru and G. D. Cismaru, in 1st International Congress on Metallic Corrosion (Butterworths, London, 1961), Chap. III, 8, p. 237.

3. P. J. Jorgensen, J. Chem. Phys., 37, 874 (1962).

4. P. J. Jorgensen, J. Chem. Phys., 49, 1594 (1968).

5. S. J. Laverty and W. D. Ryan, Int. J. Electronics, 26, 519 (1969).

6. P. J. Jorgensen, J. Electrochem. Soc., 110, 461 (1963).

7. D. H. Bradhurst, J. E. Draley and C. J. Van Drunen, J. Electrochem. Soc., 112, 1171 (1965).

8. J. B. Berkowitz-Mattuck, J. M. Ketteringham and W. P. Menashi, U.S. Nat. Tech. Inform. Serv., AD Rep., 728825, (1971), 43 pp. Avail. NTIS from Govt. Rep. Announce. (U.S.), 71, 85 (1971).

9. J. R. Anderson and I. M. Ritchie, Proc. Roy. Soc. (London), A299, 371 (1967).

10. G. L. Hunt and I. M. Ritchie, Oxid. Metals, 2, 361 (1970).

11. I. M. Ritchie, G. H. Scott and P. J. Fensham, Surface Sci., 19, 230 (1970).

12. P. K. Krishnamoorthy and S. C. Sircar, Acta Met., 16, 1461 (1968).

13. N. F. Mott and N. Cabrera, Rep. Prog. Phys., 12, 163 (1948-1949).

14. D. O. Raleigh, J. Electrochem. Soc., 113, 782 (1966).

15. P. J. Jorgensen, J. Electrochem. Soc., 114, 820 (1967).

16. D. O. Raleigh, J. Electrochem. Soc., 115, 111 (1968).

17. R. Brückner, J. Non-Crystalline Solids, 5, 177 (1971).

18. G. H. Frischat, Glastech. Ber., 45, 309 (1972).

19. A. T. Fromhold, Jr., J. Phys. Chem. Solids, 24, 1081 (1963).

20. A. T. Fromhold, Jr., J. Phys. Chem. Solids, 24, 1309 (1963).

21. A. T. Fromhold, Jr., J. Phys. Chem. Solids, 33, 95 (1972).

22. J. R. Anderson and I. M. Ritchie, Proc. Roy. Soc. (London), A299, 354 (1967).

23. F. A. Kröger, The Chemistry of Imperfect Crystals (North Holland Publ., Amsterdam, 1964).

24. C. Wagner, "Considerations on the effect of an external field applied to an oxide layer growing on a metal in oxygen," Max-Planck Institute für Physikalische Chemie, Göttingen, Germany, Unpublished memo (1966).

25. P. J. Jorgensen, in Oxidation of Metals and Alloys (American Society for Metals, Metals Park, Ohio, 1971), Chap. 9, p. 157.

26. C. Wagner, Z. Physik. Chem. (Leipzig), B21, 25 (1933).

27. L. Heyne, N. M. Beekmans and A. de Beer, J. Electrochem. Soc., 119, 77 (1972).

28. F. J. Norton, in Transactions of the 8th Vacuum Symposium and 2nd International Congress (Pergamon Press, New York, 1962), p. 8.

29. E. L. Williams, J. Am. Ceram. Soc., 48, 190 (1965).

30. B. E. Deal and A. S. Grove, J. Appl. Phys., 36, 3770 (1965).

31. C. Wagner, Z. Physik. Chem. (Leipzig), B32, 447 (1936).

32. K. Hauffe, Oxidation of Metals (Plenum Press, New York, 1965).

33. N. S. Choudhury and J. W. Patterson, J. Electrochem. Soc., 118, 1398 (1971).

34. C. Wagner, Proc. Int. Comm. Electrochem. Thermo. Kinetics (CITCE), 7, 361 (1957).

35. C. Tubandt and S. Eggert, Z. Anorg. Allgem. Chem., 110, 96 (1920).

36. J. B. Wagner and C. Wagner, J. Electrochem. Soc., 104, 509 (1957).

37. C. Tubandt, H. Reinhold and W. Jost, Z. Physik. Chem. (Leipzig), A129, 69 (1927).

38. D. O. Raleigh, J. Phys. Chem. Solids, 26, 329 (1965).

39. C. Tubandt, E. Rindtorff and W. Jost, Z. Anorg. Allgem. Chem., 165, 195 (1927).

40. J. B. Wagner and C. Wagner, J. Chem. Phys., 26, 1597 (1957).

41. J. W. Hinze and J. W. Patterson, "Electrolytic Behavior of CaF_2 Crystals under Reducing Conditions," accepted for publication in J. Electrochem. Soc., Jan. 1973.

42. N. S. Choudhury and J. W. Patterson, "Mixed Conduction in Nominally Pure Thoria," submitted to J. Am. Ceram. Soc. for publication, 1972.

43. J. Fisher and J. Bingle, J. Am. Chem. Soc., 77, 6511 (1955).

44. C. Wagner, Z. Physik. Chem. (Leipzig), B32, 447 (1936).

45. T. Dunn, G. Hetherington and K. H. Jack, Phys. Chem. Glasses, 6, 16 (1965).

46. A. G. Revez and R. J. Evans, J. Phys. Chem. Solids, 30, 551 (1969).

47. F. A. Kröger and H. J. Vink, Solid State Physics, 3, 307 (1956).

48. C. Tubandt, Z. Anorg. Allgem. Chem., 115, 105 (1920).

49. A. E. Owen and R. W. Douglas, J. Soc. Glass Tech., 43, 159 (1959).

50. P. J. Jorgensen and F. J. Norton, in VII International Congress on Glass (Gordon and Breach, New York, 1966), Paper 310.

51. K. Motzfeldt, Acta Chem. Scand., 18, 1596 (1964).

52. R. A. Rapp and D. A. Shores, in Techniques of Metals Research IV Part 2, edited by R. A. Rapp (Wiley-Interscience Publ., New York, 1970), Chap. 6C, p. 123.

53. A. G. Revez, IEEE Trans. Electron Devices, 12, 97 (1965).

54. J. W. Patterson, in Physics of Electronic Ceramics Part A, edited by L. L. Hench and D. B. Dove (Marcel Dekker, Inc., New York, 1971), Chap. 5, p. 131.

55. H. Schmaltzried, Z. Physik. Chem. (Frankfurt), 38, 87 (1963).

56. G. C. Wood, in Techniques of Metals Research IV Part 2, edited by R. A. Rapp (Wiley-Interscience Publ., New York, 1970), Chap. 10A, p. 493.

57. JANAF Thermochemical Data, Dow Corning Co., Midland, Michigan, December 31, 1960.

58. M. Hansen, Constitution of Binary Alloys (McGraw-Hill Book Co., New York, 1958), 2nd ed.

59. N. Klein, Adv. Electron. Electron Physics, 26, 309 (1969).

60. E. H. Snow and B. E. Deal, J. Electrochem. Soc., 113, 263 (1966).

61. K. N. Karube, K. Yamamoto and M. Kamiyama, Japan J. Appl. Phys., 2, 11 (1963).

62. S. W. Kurnick, J. Chem. Phys., 20, 218 (1952).

APPENDIX A. GENERAL SOLUTION FOR t = t(r) FOR THE GALVANOSTATIC CASE

The procedure for obtaining t = t(r) is to eliminate $\dot{L}$ and L from the kinetic equations in favor of r. For example solving Eq. [21] for L in terms of r and I_T results in the following expression:

$$L = -\frac{A}{I_T}\int_{\mu'_{X_2}}^{\mu''_{X_2}} \frac{[1 + r][\sigma_1 + \sigma_2]\sigma_3}{[r\sigma_3 - \sigma_1 - \sigma_2]} \frac{d\mu_{X_2}}{2z_2F} . \qquad [A\text{-}1]$$

Taking the time derivative of Eq. [A-1] we get

$$\dot{L} = \left\{\frac{A}{I_T}\int_{\mu'_{X_2}}^{\mu''_{X_2}} \frac{[\sigma_1 + \sigma_2]^2\sigma_3 + [\sigma_1 + \sigma_2]\sigma_3^2}{[r\sigma_3 - \sigma_1 - \sigma_2]} \frac{d\mu_{X_2}}{2z_2F}\right\} \frac{dr}{dt} , \qquad [A\text{-}2]$$

or more simply

$$\dot{L} = A(r)\dot{r} \qquad [A\text{-}3]$$

where A(r) is the integral expression in the braces in Eq. [A-2]. Substituting Eq. [21] into [11] we get

$$\dot{L} = \bar{v}I_T\left(\frac{r}{1 + r}\right)/FA + k_n/L. \qquad [A\text{-}4]$$

Now L can be eliminated from Eq. [A-4] by substituting in Eq. [A-1] so that

$$\dot{L} = \frac{\bar{v}I_T}{FA}\left(\frac{r}{1 + r}\right) + k_n\left\{-\frac{A}{L}\int_{\mu'_{X_2}}^{\mu''_{X_2}} \frac{[1 + r][\sigma_1 + \sigma_2]\sigma_3}{[r\sigma_3 - \sigma_1 - \sigma_2]} \frac{d\mu_{X_2}}{2z_2F}\right\}^{-1} , \qquad [A\text{-}5]$$

or

$$\dot{L} = B(r) \qquad [A\text{-}6]$$

where B(r) is the cumbersome expression for r on the right hand side of Eq. [A-5]. We may now eliminate $\dot{L}$ in favor of $\dot{r} = dr/dt$ by equating Eq. [A-3] to [A-6]. This gives

$$A(r)\,\frac{dr}{dt} = B(r) \qquad [A\text{-}7]$$

which is easily amenable to the separation of variables method. Accordingly Eq. [A-7] integrates to

$$t - t_0 = \int_{r_0}^{r} A(r)/B(r)\,dr. \qquad [A\text{-}8]$$

Of course Eq. [A-8] applies to any scaling system as long as the dependences of σ_1, σ_2 and σ_3 on μ_{X_2} are left unspecified in the integral formulas for A(r) and B(r).

APPENDIX B. DERIVATION OF THE GALVANOSTATIC SCALING KINETICS ASSUMING THE CONSTANT IONIC CONDUCTIVITY MODEL

The assumption of constant ionic conductivity, σ_{ion}, introduces major simplifications in Eq. [A-1], since now $[\sigma_1 + \sigma_2] = \sigma_{ion}$ is independent of μ_{X_2}. For example, Eq. [21] may now be written as

$$L = - \frac{A\sigma_{ion}}{I_T} \left(\frac{1 + r}{r}\right) \int_{\mu'_{X_2}}^{\mu''_{X_2}} \frac{r\sigma_3}{[r\sigma_3 - \sigma_1 - \sigma_2]} \frac{d\mu_{X_2}}{2z_2F} , \qquad [B-1]$$

or equivalently as

$$L = - \frac{A\sigma_{ion}}{I_T} \left(\frac{1 + r}{r}\right) \int_{\mu'_{X_2}}^{\mu''_{X_2}} \left\{1 + \frac{\sigma_{ion}}{[r\sigma_3 - \sigma_1 - \sigma_2]}\right\} \frac{d\mu_{X_2}}{2z_2F} \qquad [B-2]$$

where Eq. [B-2] is the sum of two integrals. The first is identically equal to $- E_{TH}$ (Eq. [17]) while the second is identical to V_T (Eq. [15]). Thus,

$$L = \frac{A\sigma_{ion}}{I_T} \left(\frac{1 + r}{r}\right) (E_{TH} - V_T). \qquad [B-3]$$

Taking the time derivatives of this expression we obtain an equation analogous to Eq. [A-3]; i.e.,

$$\dot{L} = \frac{A\sigma_{ion}}{I_T} \frac{d}{dt} \left[\left(\frac{1 + r}{r}\right) (E_{TH} - V_T)\right] \qquad [B-4]$$

where $V_T = V_T(r)$ given by Eq. [15]. Substituting Eq. [B-3] into [A-4] to eliminate L gives

$$\dot{L} = \frac{\bar{v} I_T}{FA} \left(\frac{r}{1 + r}\right) + \kappa_n \left[\frac{A\sigma_{ion}}{I_T} \left(\frac{1 + r}{r}\right) (\bar{E}_{TH} - \bar{V}_T)\right]^{-1} . \qquad [B-5]$$

Equating Eq. [B-5] to [B-4] and simplifying we get an equation of the form

$$\varphi\Delta d(\varphi\Delta)/dt = a + b\Delta \qquad [B\text{-}6]$$

where

$$\varphi = (\frac{1 + r}{r}); \; \Delta = E_{TH} - V_T; \; a = \left[\frac{I_T}{\sigma_{ion} A}\right]^2 k_n; \; b = \frac{\tilde{v}}{\sigma_{ion} F}\left[\frac{I_T}{A}\right]^2 . \qquad [B\text{-}7]$$

Solving Eq. [B-6] by separation of variables results in

$$t - t_0 = \int_{r_0}^{r} \frac{\varphi\Delta d(\varphi\Delta)}{a + b\Delta} \qquad [B\text{-}8]$$

where the integral in Eq. [B-8] may be readily solved by numerical integration techniques.

A further simplification results of the flux of neutral species is negligible in comparison to the ionic flux. Then k_n and the constant, a, in Eq. [B-6] vanish reducing Eq. [B-8] to

$$t - t_0 = \frac{1}{b} \int_{r_0}^{r} \varphi d(\varphi\Delta). \qquad [B\text{-}9]$$

Integration by parts then gives

$$2b[t - t_0] = \varphi^2\Delta \Big|_{r_0}^{r} + \int_{r_0}^{r} \varphi^2 d\Delta \qquad [B\text{-}10]$$

The forms of Δ and $d\Delta$, and hence, the interdependence of t and r, are ultimately determined by the inherent defect structure of the scaling layer involved. Once this information is put into the problem, the integrals take standard forms and we get $t = t(r)$ explicitly. Then

it is a simple matter to calculate V_T, L and t values for as many r values as may be desired. One merely inserts each r value into Eqs. [15], [B-3] and t(r) respectively. This method is necessary because of the highly complicated functions of r which generally result on the right side of [B-10]. Otherwise one could merely invert Eq. [B-8] to get r = r(t), insert the result in Eqs. [15] and [B-3], respectively, and then integrate to get $V_T(r)$ and L(r) more directly. The method will now be demonstrated by applying it to a specific system; namely, Ag, AgBr for which the necessary information is known.

Silver Bromination

Equation [B-10] will now be applied to the particular case of silver bromination. The ionic conductivity of silver bromide is known to be μ_{Br_2} independent (32) and the magnitude and μ_{Br_2} dependences of the electronic conductivity are well known (38). The galvanostatic thickening or thinning kinetics can, therefore, be readily predicted.

No neutral transport exists in AgBr so that k_n vanishes and Eq. [B-10] is applicable. Silver bromide has the Frenkel defect structure; i.e., ionic defects consist essentially of equal concentrations of silver ion interstitials and vacancies (23). Anion defect concentrations are negligible in comparison to cation defect concentrations so that $\sigma_{ion} \approx \sigma_1$. The only mobile electronic defect of significance is the positive hole whose concentration varies as $P_{Br_2}^{1/2}$ (38). Hence, σ_3 is proportional to $P_{Br_2}^{1/2}$ as follows:

$$\sigma_3 = \sigma_{ion}(P_{Br_2}/P_{\oplus})^{1/2} \qquad [B\text{-}11]$$

where $P_{\oplus}$ is the bromine pressure at which the hole conductivity is equal to the ionic conductivity. Knowledge of the pressure dependence of σ_3 allows us to integrate Eq. [B-10] to obtain the time dependence of r. The first step is to get $V_T(r)$. Using Eq. [B-11] and the fact that σ_{ion} is constant, Eq. [15] may be integrated to give

$$V_T = \frac{RT}{2F} \ell n\left[\frac{P''_{Br_2}}{P'_{Br_2}}\right] - \frac{RT}{F} \ell n\left[\frac{1 - r(P''_{Br_2}/P_{\oplus})^{1/2}}{1 - r(P'_{Br_2}/P_{\oplus})^{1/2}}\right] \qquad [B\text{-}12]$$

where the variable of integration has been changed to P_{Br_2} as follows: $\mu_{Br_2} = \mu^{o}_{Br_2} + RT\ \ell n\ P_{Br_2}$ and $d\mu_{Br_2} = RTdP_{Br_2}/P_{Br_2}$. The first term in Eq. [B-12] is identical to the thermodynamic emf, E_{TH}. Thus,

$$E_{TH} - V_T = \Delta = \frac{RT}{F} \ell n\left[\frac{1 - r(P''_{Br_2}/P_{\oplus})^{1/2}}{1 - r(P'_{Br_2}/P_{\oplus})^{1/2}}\right]. \qquad [B\text{-}13]$$

Letting $(P''_{Br_2}/P_{\oplus})^{1/2} = \beta$ and $(P'_{Br_2}/P_{\oplus})^{1/2} = \alpha$ we get

$$\Delta = \frac{RT}{F} \ell n\left[\frac{1 - r\beta}{1 - r\alpha}\right], \qquad [B\text{-}14]$$

and

$$d\Delta = \frac{RT}{F}\left[\frac{\alpha}{1 - r\alpha} - \frac{\beta}{1 - r\beta}\right]dr. \qquad [B\text{-}15]$$

Substituting Eq. [B-14] and [B-15] into [B-10] and remembering that $\varphi = \left(\frac{1 + r}{r}\right)$ we get

$$2b[t - t_0] = \frac{RT}{F}\left(\frac{1 + r}{r}\right)^2 \ell n\left[\frac{1 - r\beta}{1 - r\alpha}\right]\Bigg|_{r_0}^{r} + \frac{RT}{F}\int_{r_0}^{r}\left(\frac{1 + r}{r}\right)^2 \cdot \left[\frac{\alpha}{1 - r\alpha} - \frac{\beta}{1 - r\beta}\right]dr. \qquad [B\text{-}16]$$

This is equivalent to

$$t - t_0 = \frac{RT}{2bF}\left\{\left[\left(\frac{1+r}{r}\right)^2 + 1\right]\ell n\left[\frac{1-r\beta}{1-r\alpha}\right] + \left[2\beta + \beta^2\right]\ell n\left[\frac{1-r\beta}{r}\right] + \left[2\alpha + \alpha^2\right]\ell n\left[\frac{1-r\alpha}{r}\right] + \left[\frac{\beta-\alpha}{r}\right]\right\}_{r_0}^{r} \qquad [B\text{-}17]$$

where r_0 is the value of r at $t = t_0$. The value for r_0 is determined by rewriting Eq. [B-3] as

$$L_0 = \frac{ART\sigma_{ion}}{I_T F}\left(\frac{1+r_0}{r_0}\right)\ell n\left[\frac{1-r_0\beta}{1-r_0\alpha}\right];\ t = t_0, \qquad [B\text{-}18]$$

and solving for r_0 by numerical techniques for given values of I_T and L_0. Substituting the value of r_0 into Eq. [B-17] gives the time dependence of r. Similarly, for $t > t_0$ Eqs. [B-3], [B-13] and [B-14] combine to give

$$L = \frac{ART\sigma_{ion}}{I_T F}\left(\frac{1+r}{r}\right)\ell n\left[\frac{1-r\beta}{1-r\alpha}\right];\ t > t_0. \qquad [B\text{-}19]$$

Thus, Eq. [B-19] may be used in conjunction with Eq. [B-17] to determine the time dependence of the scale thickness. The time dependence of V_T may be obtained by using Eq. [B-12] in conjunction with Eq. [B-17]. Accelerated growth will be predicted when $r < -1$ or $V_T < E_W$; retarded growth when $-1 < r < 0 + \delta$ or $E_W < V_T < V_{Halt}$ and decomposition or scale thinning when $r > 0 + \delta$ or $V_T > V_{Halt}$ where δ is an indication of the amount of neutral transport through the scale.

The procedure for predicting the galvanostatic thickening or thinning kinetics of silver bromide can be summarized as follows:

1) Determine the magnitudes of σ_{ion}, $P_{\oplus}$, α and β used in the computations. Values of these parameters can be easily obtained for AgBr.

2) Determine r_0 from Eq. [B-18] for a given set of I_T, L_0 experimental conditions. 3) Increment r from r_0 to the desired final value. 4) Calculate the corresponding values of $t - t_0$, V_T and L from Eqs. [B-17], [15] and [B-3] which are all parametric in r. 5) One may then plot L and V_T versus the calculated values of $t - t_0$.

A Fortran computer program illustrating this technique for silver bromination and using the conductivity data of Kurnick (62) and Raleigh (38) is given in Appendix E.

APPENDIX C. DERIVATIONS OF THE GALVANOSTATIC AND POTENTIOSTATIC SCALING KINETICS ASSUMING THE CONSTANT IONIC TRANSFERENCE NUMBER MODEL

Galvanostatic Scaling Kinetics

An alternate expression for Eq. [11] can be derived in which the parameter r is absent. For example, if the identity $t_{ion} + t_3 = 1$ is inserted into Eq. [8] we obtain

$$\dot{n} = t_{ion}I_T/F + t_3I_T/F + \frac{A\sigma_3[\sigma_1 + \sigma_2]}{[r\sigma_3 - \sigma_1 - \sigma_2]} \frac{\nabla\mu_{X_2}}{2z_2F} + 2z_2AJ_{X_2}/N. \qquad [C\text{-}1]$$

We can eliminate I_T from the second term in Eq. [C-1] by inserting the differential equation form of Eq. [21]. Doing this we get

$$\dot{n} = t_{ion}I_T/F - \frac{A\sigma_3}{[\sigma_1 + \sigma_2 + \sigma_3]} \frac{[1 + r]\sigma_3[\sigma_1 + \sigma_2]}{[r\sigma_3 - \sigma_1 - \sigma_2]} \frac{\nabla\mu_{X_2}}{2z_2F^2} + \frac{A\sigma_3[\sigma_1 + \sigma_2]}{[r\sigma_3 - \sigma_1 - \sigma_2]} \frac{\nabla\mu_{X_2}}{2z_2F^2} + 2z_2AJ_{X_2}/N. \qquad [C\text{-}2]$$

Collecting coefficients on $\nabla\mu_{X_2}$ and then integrating over the scale thickness we get

$$\dot{n} = \frac{I_T}{FL}\int_0^L t_{ion}d\ell - \frac{A}{L}\left\{\int_{\mu'_{X_2}}^{\mu''_{X_2}} \frac{\sigma_3[\sigma_1 + \sigma_2]}{[\sigma_1 + \sigma_2 + \sigma_3]} \frac{d\mu_{X_2}}{2z_2F^2} + 2z_2D_{X_2}\Delta C_{X_2}/N\right\}, \qquad [C\text{-}3]$$

and substituting Eq. [10] into [C-3] gives

$$\dot{L} = \frac{\bar{v}I_T}{FLA}\int_0^L t_{ion}d\ell - \frac{\bar{v}}{L}\left\{\int_{\mu'_{X_2}}^{\mu''_{X_2}} \frac{\sigma_3[\sigma_1 + \sigma_2]}{[\sigma_1 + \sigma_2 + \sigma_3]} \frac{d\mu_{X_2}}{2z_2F^2} + 2z_2D_{X_2}\Delta C_{X_2}/N\right\}. \qquad [C\text{-}4]$$

The second term in Eq. [C-4] is identical to Wagner's scaling rate constant (Figure 2) divided by L whence,

$$\dot{L} = \frac{\bar{v}I_T}{FLA}\int_0^L t_{ion}d\ell + [k + k_n]/L. \qquad [C\text{-}5]$$

Equation [C-5] is identical to Eq. [1] derived by Kröger (23) where the integral in the first term divided by L is $\bar{t}_{ion}$. This equation was not derived for the general case because t_{ion} in the integral is, in general, strongly dependent on μ_{X_2}. The internal μ_{X_2} profile must change with time because L, r and V_T are also changing. In effect this buries the time variable inside the integral term in Eq. [C-5] thus precluding separation of the variables L and t. For this reason the alternative method of eliminating the parameter r amongst t(r), $V_T(r)$ and L(r) was used for analyzing the general galvanostatic case as well as the constant ionic conductivity case.

For the constant t_{ion} case, however, t_{ion} is μ_{X_2} independent and, therefore, independent of location in the scale as well. Thus, Eq. [C-5] simplifies to

$$\dot{L} = \bar{v}I_T t_{ion}/FA + [k + k_n]/L \qquad [C\text{-}6]$$

where t_{ion} is constant independent of μ_{X_2}, L and, therefore, time. Note that if $\dot{L}$ in Eq. [C-6] is zero, the electrolysis rate given by the first term just balances the diffusional fluxes of the second term. Equation [C-6] may then be solved for the final or steady state thickness, L_∞, corresponding to $\dot{L} = 0$. When this is done, L_∞ is given by $-[k + k_n]/c$ where c is equal to the first term in Eq. [C-6]

and is the rate at which the scale is being electrolyzed by an impressed current.

Since the first term in Eq. [C-6] is totally constant with time, Eq. [C-6] integrates to

$$t - t_0 = \frac{1}{c}\left\{L - L_0 + L_\infty \ell n\left[\frac{L_\infty - L}{L_\infty - L_0}\right]\right\} . \qquad [C\text{-}7]$$

Equation [C-6] and [C-7] will predict accelerated growth, retarded growth or thinning of the scaling layer depending on the magnitude and sign of the total current.

It is now desirable to get an equation for the time dependence of the voltage since voltage can be measured in situ. The method of eliminating r from $V_T(r)$ and $t(r)$ could again be used; however, a much more direct approach is now possible. This involves the development of an alternative equation for V_T. Inserting the fundamental formulas for I_1, I_2 and I_3 (in terms of electrochemical potential gradients and conductivities) into Eq. [3] and then using Wagner's local equilibrium equations (Figure 2) one may derive the equation

$$\frac{\nabla\eta_3}{z_3F} = -\frac{[\sigma_1 + \sigma_2]}{[\sigma_1 + \sigma_2 + \sigma_3]}\frac{\nabla\mu_{X_2}}{2z_2F} - \frac{I_T}{[\sigma_1 + \sigma_2 + \sigma_3]A} , \qquad [C\text{-}8]$$

and integrating Eq. [C-8] yields

$$V_T = E_W - \frac{I_T}{A}\int_0^L \frac{d\ell}{\sigma_1 + \sigma_2 + \sigma_3} . \qquad [C\text{-}9]$$

In order to obtain a quantitative expression for V_T, it is necessary to evaluate the integral in Eq. [C-9]. In general, each σ_j in Eq. [C-9] is known as a function of μ_{X_2} or P_{X_2} but not as a function of ℓ. What is required in this case is a knowledge of the chemical potential

profile in the scale; i.e., $\mu_{X_2} = \mu_{X_2}(\ell)$ or $P_{X_2} = P_{X_2}(\ell)$ so that we can eliminate $d\ell$ in favor of $d\mu_{X_2}$ or dP_{X_2}. This can be done by dividing the differential equation form of Eq. [21] by [21] and assuming that steady state prevails at each location in the scaling layer so that

$$\frac{d\ell}{L} = \frac{[\sigma_1 + \sigma_2]\sigma_3 d\mu_{X_2}}{[r\sigma_3 - \sigma_1 - \sigma_2]} \Big/ \int_{\mu'_{X_2}}^{\mu''_{X_2}} \frac{[\sigma_1 + \sigma_2]\sigma_3 d\mu_{X_2}}{[r\sigma_3 - \sigma_1 - \sigma_2]} \qquad [C\text{-}10]$$

or equivalently

$$\frac{d\ell}{L} = \frac{[\sigma_1 + \sigma_2]\sigma_3 dP_{X_2}}{[r\sigma_3 - \sigma_1 - \sigma_2]P_{X_2}} \Big/ \int_{P'_{X_2}}^{P''_{X_2}} \frac{[\sigma_1 + \sigma_2]\sigma_3 dP_{X_2}}{[r\sigma_3 - \sigma_1 - \sigma_2]P_{X_2}} \qquad [C\text{-}11]$$

In order for t_{ion} to be independent of P_{X_2} each σ_j must have the same P_{X_2} dependence. To prove this we can write

$$t_{ion} = t_1 + t_2 = \frac{\sigma_1 + \sigma_2}{\sigma_1 + \sigma_2 + \sigma_3} = \frac{\sigma_1^o P_{X_2}^{1/n} + \sigma_2^o P_{X_2}^{1/n}}{\sigma_1^o P_{X_2}^{1/n} + \sigma_2^o P_{X_2}^{1/n} + \sigma_3^o P_{X_2}^{1/n}} \qquad [C\text{-}12]$$

where σ_j^o is the conductivity of the jth specie at $P_{X_2} = 1$ atm, and n is a positive or negative integer. Thus, cancelling the factor $P_{X_2}^{1/n}$ yields

$$t_{ion} = \frac{\sigma_1^o + \sigma_2^o}{\sigma_1^o + \sigma_2^o + \sigma_3^o}, \qquad [C\text{-}13]$$

and t_{ion} is indeed constant. Inserting each σ_j^o into Eq. [C-11] results in the equation

$$\frac{d\ell}{L} = [P_{X_2}^{1/n} dP_{X_2}/P_{X_2}] \Big/ \int_{P'_{X_2}}^{P''_{X_2}} P_{X_2}^{1/n} dP_{X_2}/P_{X_2} , \qquad [C\text{-}14]$$

which is independent of r. Thus we have a formula for obtaining $d\ell$ in terms of dP_{X_2}. Whence

$$\frac{d\ell}{L} = \frac{P_{X_2}^{1/n} dP_{X_2}}{n(\Delta P_{X_2}^{1/n}) P_{X_2}} \qquad [C\text{-}14a]$$

where $(\Delta P_{X_2}^{1/n}) = P''^{1/n}_{X_2} - P'^{1/n}_{X_2}$. Now we can eliminate $d\ell$ in Eq. [C-9] for dP_{X_2} so that Eq. [C-9] becomes

$$V_T = E_W - \frac{I_T L}{nA(\Delta P_{X_2}^{1/n})} \int_{P'_{X_2}}^{P''_{X_2}} \frac{P_{X_2}^{(1/n-1)} dP_{X_2}}{[\sigma_1 + \sigma_2 + \sigma_3]} . \qquad [C\text{-}15]$$

Carrying out the integration in Eq. [C-15] we get

$$V_T = E_W - \frac{I_T L \, \ell n[P''_{X_2}/P'_{X_2}]}{nA(\Delta P_{X_2}^{1/n})[\sigma_1^o + \sigma_2^o + \sigma_3^o]} \qquad [C\text{-}16]$$

where $\sigma_j = \sigma_j^o P_{X_2}^{1/n}$. Remembering from Eq. [17] that

$$E_{TH} = -[\mu''_{X_2} - \mu'_{X_2}]/2z_2F = -\frac{RT}{2z_2F} \ell n[P''_{X_2}/P'_{X_2}] \qquad [C\text{-}17]$$

we get finally that

$$V_T = E_W + \frac{2z_2FE_{TH}I_TL}{nART\sigma_T^o(\Delta P_{X_2}^{1/n})} . \qquad [C\text{-}18]$$

where $\sigma_T^o = \sigma_1^o + \sigma_2^o + \sigma_3^o$. Equation [C-18] may be written as

$$V_T = E_W - \frac{I_T L}{\sigma_T A} \qquad [C\text{-}19]$$

where

$$\bar{\sigma}_T = - \frac{nRT\sigma_T^o(\Delta P_{X_2}^{1/n})}{2z_2FE_{TH}} . \qquad [C\text{-}20]$$

All of the parameters in Eq. [C-18] can, in principle, be measured. Thus, by obtaining the time dependence of L from Eq. [C-7] allows us to calculate the time dependence of V_T from Eq. [C-19].

Potentiostatic Scaling Kinetics

For the constant t_{ion} model it was shown that it is convenient to use Eq. [C-6] instead of Eq. [11] for $\dot{L}$ because of the way in which the parameter r drops out of the analysis. Likewise a more convenient form of Eq. [24] for the scaling kinetics under potentiostatic conditions may be derived in which r is absent. For example, if we solve Eq. [C-18] for I_T and substitute the resulting expression into Eq. [C-6], we get

$$\dot{L} = \left\{ \frac{\bar{v}nRTt_{ion}\sigma_T^o(V_T - E_W)(\Delta P_{X_2}^{1/n})}{2z_2F^2E_{TH}} + k + k_n \right\} /L. \qquad [C\text{-}21]$$

Integrating Eq. [C-21] we obtain

$$L^2 = L_0^2 + 2\left\{ \frac{\bar{v}nRTt_{ion}\sigma_T^o(V_T - E_W)(\Delta P_{X_2}^{1/n})}{2z_2F^2E_{TH}} + k + k_n \right\} \cdot [t - t_0]. \qquad [C\text{-}22]$$

From Eq. [C-22] it can be easily seen that the scale thickening or thinning is parabolic. When $V_T < E_W$, accelerated growth will be exhibited; $V_T > E_W$, retarded growth; and scale thinning will be exhibited when the first term in the braces is greater than $k + k_n$.

Normal oxidation will occur when $V_T = E_W$. In this case the first term in Eq. [C-22] vanishes. Substituting Eq. [C-22] into Eq. [C-18] and rearranging results in the following expression for I_T^{-2}:

$$I_T^{-2} = \left\{\frac{2z_2FE_{TH}L_0}{nART\sigma_T^o(\Delta P_{X_2}^{1/n})(V_T - E_W)}\right\}^2 + 2\left\{\left[\frac{2z_2\bar{v}E_{TH}t_{ion}}{nA^2RT\sigma_T^o(\Delta P_{X_2}^{1/n})(V_T - E_W)}\right] + \left[\frac{2z_2FE_{TH}}{nART\sigma_T^o(\Delta P_{X_2}^{1/n})(V_T - E_W)}\right]^2[k + k_n]\right\}[t - t_0]. \quad [C\text{-}23]$$

Thus, a plot of I_T^{-2} versus $t - t_0$ gives a straight line with the slope and intercept given in Eq. [C-23]. Again, each of the parameters in Eq. [C-23] can, in principle, be measured experimentally.

APPENDIX D. TWO GENERAL TRANSPORT MODELS FOR PREDICTING THE EFFECT OF APPLIED ELECTRIC FIELDS ON SILICON OXIDATION

In what follows two general defect models are considered for the description of mass and charge transport in SiO_2. These models are used to predict the kinetics of thickening and thinning of SiO_2 films for potentiostatic and galvanostatic conditions. In order to predict these kinetics, it is necessary to first derive relationships for certain of the parameters used in the subsequent calculations in terms of measurable quantities; namely, k and E_W. This is because values for σ_T^o, the value of the total conductivity at one atmosphere oxygen pressure and σ_{ion}, the value of the ionic conductivity are unknown for SiO_2 at the present time. Thus, relationships are derived for these parameters below.

Constant Ionic Transference Number Model

Consider oxygen incorporation into the SiO_2 network by the following reaction:

$$\frac{1}{2} O_2(g) = O_i'' + 2h \qquad [D\text{-}1]$$

where O_i'' is a divalent oxygen interstitial and h is a positive hole. From the law of mass action

$$\frac{[O_i''] p^2}{P_{O_2}^{1/2}} = K. \qquad [D\text{-}2]$$

For the constant t_{ion} model charge neutrality requires that

$$2[O_i''] = p \qquad [D-3]$$

where p is the concentration of holes. Inserting Eq. [D-3] into [D-2] we get that

$$p, [O_i''] \propto P_{O_2}^{1/6} . \qquad [D-4]$$

But conductivity is related to concentration by

$$\sigma_j = q_j^2 C_j B_j \qquad [D-5]$$

where σ_j, q_j, C_j and B_j are, respectively, the conductivity, charge, concentration and absolute mobility of the jth species. Whence,

$$\sigma_2 = q_2^2[O_i'']B_2; \quad \sigma_3 = q_3^2 p B_3 \qquad [D-6]$$

where the subscripts 2 and 3 have their usual meaning. We may substitute Eq. [D-4] into [D-6] to obtain

$$\sigma_2 \propto P_{O_2}^{1/6} \quad \text{or} \quad \sigma_2 = \sigma_2^o P_{O_2}^{1/6} , \qquad [D-7]$$

$$\sigma_3 \propto P_{O_2}^{1/6} \quad \text{or} \quad \sigma_3 = \sigma_3^o P_{O_2}^{1/6} , \qquad [D-8]$$

and

$$\sigma_T = \sigma_2 + \sigma_3 \quad \text{or} \quad \sigma_T = \sigma_T^o P_{O_2}^{1/6} \qquad [D-9]$$

where σ_j^o is the conductivity of the jth species at P_{O_2} = 1 atm. Now $t_{ion} = \sigma_{ion}/\sigma_T$ so that it can easily be seen that t_{ion} is P_{O_2} or equivalently μ_{O_2} independent.

We proceed to derive an expression for σ_T^o as follows. From

Figure 2

$$E_W = -\int_{\mu'_{X_2}}^{\mu''_{X_2}} \frac{[\sigma_1 + \sigma_2]}{[\sigma_1 + \sigma_2 + \sigma_3]} \frac{d\mu_{X_2}}{2z_2F} = -\int_{\mu'_{X_2}}^{\mu''_{X_2}} t_{ion} \frac{d\mu_{X_2}}{2z_2F} \quad [D\text{-}10]$$

For the constant t_{ion} model Eq. [D-10] reduces to

$$E_W = t_{ion} \int_{\mu'_{O_2}}^{\mu''_{O_2}} \frac{d\mu_{O_2}}{4F} = t_{ion} E_{TH} \quad [D\text{-}11]$$

where $2z_2 = -4$ for SiO_2. Equation [D-11] may be written as

$$t_{ion} = E_W/E_{TH} . \quad [D\text{-}12]$$

This equation for t_{ion} is exact and not an average value. From Figure 2

$$k = -\bar{v} \int_{\mu'_{X_2}}^{\mu''_{X_2}} \frac{\sigma_3[\sigma_1 + \sigma_2]}{[\sigma_1 + \sigma_2 + \sigma_3]} \frac{d\mu_{X_2}}{2z_2F^2} . \quad [D\text{-}13]$$

Again, for SiO_2, $2z_2 = -4$ and $d\mu_{O_2} = RTdP_{O_2}/P_{O_2}$. Thus,

$$k = \frac{\bar{v}RT}{4F^2} \int_{P'_{O_2}}^{P''_{O_2}} \frac{\sigma_2\sigma_3}{\sigma_T} \frac{dP_{O_2}}{P_{O_2}} . \quad [D\text{-}14]$$

where $\sigma_1 \approx 0$. Substitution of Eq. [D-9] into [D-4] allows us to write

$$k = \frac{\bar{v}RTt_{ion}t_3}{4F^2} \int_{P'_{O_2}}^{P''_{O_2}} \sigma_T^o P_{O_2}^{1/6} \frac{dP_{O_2}}{P_{O_2}} \quad [D\text{-}15]$$

where t_{ion} is P_{O_2} independent and $t_3 = 1 - t_{ion}$. Equation [D-15] may be integrated to give

$$k = \frac{3\bar{v}RTt_{ion}t_3\sigma_T^o(\Delta P_{O_2}^{1/6})}{2F^2} . \qquad [D\text{-}16]$$

Solving Eq. [D-16] for σ_T^o we get

$$\sigma_T^o = \frac{2kF^2}{3\bar{v}RTt_{ion}t_3(\Delta P_{O_2}^{1/6})} . \qquad [D\text{-}17]$$

We substitute Eq. [D-12] into [D-17] to obtain finally that

$$\sigma_T^o = \frac{2F^2E_{TH}^2k}{3\bar{v}RTE_W(E_{TH} - E_W)(\Delta P_{O_2}^{1/6})} \qquad [D\text{-}18]$$

where k is the ionic part of the scaling rate constant. However, on the strength of the electrolytic decomposition experiments of this work and previous observations of the halt voltage (3, 4) it is concluded that k is the total scaling rate constant given by 1.25×10^{-11} cm^2/h at 850 °C. Thus, Eq. [D-18] for σ_T^o is in terms of measurable quantities; namely, E_W and k. Equation [D-18] can be used in conjunction with Eqs. [C-18] and [C-7] to obtain the galvanostatic scale thickening and thinning kinetics; and in conjunction with Eqs. [C-22] and [C-23] to obtain the potentiostatic kinetics for SiO_2 films. A Fortran computer program for calculating the galvanostatic scaling kinetics of silicon in oxygen gas assuming the constant t_{ion} model is presented in Appendix F.

Constant Ionic Conductivity Model

A similar calculation can be made for the assumption of a constant σ_{ion} model. In this case the oxygen incorporation reaction of

Eq. [D-1] is the same along with the law of mass action, Eq. [D-2]. However, now it must be assumed that a significant number of oxygen ion vacancies exist in the SiO_2 network. Now the charge neutrality condition becomes

$$2[O_i''] = 2[V_O^{\cdot\cdot}] + p \qquad [D\text{-}19]$$

where $V_O^{\cdot\cdot}$ is a divalent oxygen ion vacancy. The concentrations of oxygen interstitials and vacancies are assumed to be large in comparison to the concentration of holes and nearly equal so that p in Eq. [D-19] is small. Thus, it is assumed that $[O_i'']$ is P_{O_2} independent so that the law of mass action becomes

$$p = K' P_{O_2}^{1/4} . \qquad [D\text{-}20]$$

Since conductivity is proportional to concentration,

$$\sigma_3 \propto p \qquad \text{or} \qquad \sigma_3 = \sigma_3^o P_{O_2}^{1/4} . \qquad [D\text{-}21]$$

Similarly

$$\sigma_{ion} \propto [O_i''] \qquad \text{or} \qquad \sigma_{ion} = \text{const.} \qquad [D\text{-}22]$$

It is convenient to write Eq. [D-21] as

$$\sigma_3 = \sigma_{ion} P_{\oplus}^{-1/4} P_{O_2}^{1/4} \qquad [D\text{-}23]$$

where $P_{\oplus}$ is the oxygen pressure at which $\sigma_3 = \sigma_{ion}$.

Now we proceed in the same way as before only now a relationship for σ_{ion} is sought. Equation [D-10] for E_w becomes

$$E_W = \frac{RT}{4F} \int_{P'_{O_2}}^{P''_{O_2}} \frac{\sigma_{ion}}{[\sigma_{ion} + \sigma_3]} \frac{dP_{O_2}}{P_{O_2}} . \qquad [D\text{-}24]$$

Substituting Eq. [D-23] into [D-24] and then integrating we obtain

$$E_W = E_{TH} - \frac{RT}{F} \ell n \left[\frac{1 + (P''_{O_2}/P_\oplus)^{1/4}}{1 + (P'_{O_2}/P_\oplus)^{1/4}} \right] . \qquad [D\text{-}25]$$

Solving Eq. [D-25] for $P_\oplus^{-1/4}$ gives

$$P_\oplus^{-1/4} = \frac{\exp\left[\frac{(E_{TH} - E_W)F}{RT}\right] - 1}{P''^{1/4}_{O_2} - P'^{1/4}_{O_2} \exp\left[\frac{(E_{TH} - E_W)F}{RT}\right]} . \qquad [D\text{-}26]$$

Thus, knowing E_W allows us to calculate $P_\oplus^{-1/4}$.

Equation [D-13] for k becomes

$$k = \frac{\bar{v}RT}{4F^2} \int_{P'_{O_2}}^{P''_{O_2}} \frac{\sigma_{ion}\sigma_3}{[\sigma_{ion} + \sigma_3]} \frac{dP_{O_2}}{P_{O_2}} . \qquad [D\text{-}27]$$

Again, substituting Eq. [D-23] into [D-27] and then integrating yields

$$k = \frac{\bar{v}RT\sigma_{ion}}{F^2} \ell n \left[\frac{1 + \beta'}{1 + \alpha'} \right] \qquad [D\text{-}28]$$

where $\alpha' = (P'_{O_2}/P_\oplus)^{1/4}$; $\beta' = (P''_{O_2}/P_\oplus)^{1/4}$. Thus, we get for σ_{ion}

$$\sigma_{ion} = \frac{kF^2}{\bar{v}RT} \left\{ \ell n \left[\frac{1 + \beta'}{1 + \alpha'} \right] \right\}^{-1} \qquad [D\text{-}29]$$

where the quantities on the right hand side of Eq. [D-29] are all known. Substitution of Eqs. [D-22] and [D-23] into Eq. [15] and then integrating gives the cell voltage

$$V_T = E_{TH} - \frac{RT}{F} \ell n[\frac{1 - r\beta'}{1 - r\alpha'}]. \qquad [D\text{-}30]$$

The thickness L is given by Eq. [B-3]; i.e.,

$$L = \frac{A\sigma_{ion}}{I_T} (\frac{1 + r}{r}) (E_{TH} - V_T) \qquad [B\text{-}3]$$

where σ_{ion} is given by Eq. [D-29], and V_T is given by Eq. [D-30]. Now all that is required to predict the galvanostatic scaling kinetics is an equation for the time dependence of the parameter r. Equation [B-10] can again be used to obtain t(r) directly since k_n is zero. Thus, an equation results which is the same form as Eq. [B-17] except that now $\alpha \rightarrow \alpha'$ and $\beta \rightarrow \beta'$.

For potentiostatic scaling kinetics, of course, parabolic growth or decomposition will always be exhibited. All that is required is a knowledge of k(r) in Eqs. [25] and [29]. For the constant ionic conductivity model Eq. [13] for k(r) becomes simply

$$k(r) = \frac{\bar{v}\sigma_{ion}}{F} (E_{TH} - V_T). \qquad [D\text{-}31]$$

Thus, by knowing the scaling rate constant of silicon, k, and the open circuit emf, E_W, the kinetics of scale thickening and thinning for SiO_2 under various potentiostatic and galvanostatic conditions can be calculated. A Fortran computer program for calculating the galvanostatic scaling kinetics of silicon in oxygen gas assuming the constant σ_{ion} model is given in Appendix G.

APPENDIX E. FORTRAN COMPUTER PROGRAM FOR CALCULATING THE GALVANOSTATIC SCALING KINETICS OF SILVER IN BROMINE GAS

```
//D201JH23  JOB  'U3191,TIME=3,SIZE=128K',HINZE
//STEP1  EXEC  WATFIV,REGION.GO=128K
//GO.SYSIN  DD  *
$JOB            U3191HINZE,TIME=07,PAGES=40
C      THIS PROGRAM CALCULATES THE GALVANOSTATIC SCALING KINETICS OF
C      SILVER IN BROMINE GAS. THE CONSTANT IONIC CONDUCTIVITY MODEL IS
C      ASSUMED FOR THE CALCULATION.
       REAL*8 PR,PL,PPOS,EW,ETH,F,FF,DEXP,RG,TK,BETA,SIGI,A,B,DLOG,E,R,RO
      1,VOL,AREA,X,T,AMPS,CONST,DELTA,SCLRT,C,DR,D,FUNC,DEL,Z,DABS,XOC,RA
      2TE,DSQRT,ROO,FX,FFX,SIGH
       RG=1.987
       FF=96500.
       F=23062.
       TK=623.
       VOL=29.
       AREA=1.
       PL=10.**(5.10-11670/TK)
       PR=0.08292
       ETH=(RG*TK/(2.*F))*DLOG(PR/PL)
       SIGI=10.**(-1.)
       SIGH=10.**(-3.)
       PPOS=(SIGI/SIGH)**2.
       A=(PL/PPOS)**0.50
       B=(PR/PPOS)**0.50
       BETA=DLOG((1.+B)/(1.+A))
       EW=ETH-RG*TK*BETA/F
C      RG IS THE GAS CONSTANT, FF AND F ARE, RESPECTIVELY, THE FARADAY
C      NUMBER IN COUL/EQ AND CAL/VOLT EQ, TK IS THE ABSOLUTE TEMPERATURE,
C      VOL IS THE EQUIVALENT VOLUME, PL IS THE BROMINE PRESSURE AT THE
C      AG,AGBR INTERFACE, PR IS THE BROMINE PRESSURE AT THE AGBR,BR2
C      INTERFACE, ETH IS THE THERMODYNAMIC EMF, SIGI IS THE IONIC
C      CONDUCTIVITY, SIGH IS THE HOLE CONDUCTIVITY, PPOS IS THE BROMINE
C      PRESSURE AT WHICH THE IONIC AND HOLE CONDUCTIVITIES ARE EQUAL
C      AND EW IS THE OPEN CIRCUIT EMF.
       SCLRT=((RG*TK*SIGI)/(F*FF))*DLOG((1.+B)/(1.+A))
C      SCLRT IS THE SCALING RATE CONSTANT IN EQ/CM SEC.
       RATE=SCLRT*VOL*3600.
```

```
C     RATE IS THE SCALING RATE CONSTANT IN SQUARE CM/HR.
      READ(5,4)M
      DO 300 J=1,M
      READ(5,100)AMPS,XO,N
C     AMPS IS THE TOTAL CURRENT AND XO IS THE INITIAL THICKNESS IN
C     ANGSTROMS.
      WRITE(6,180)
      FUNC=AMPS*XO*F*(10.**(-8.))/(AREA*SIGI*RG*TK)
      L=2
   19 ROO=(1.-0.1**L)/B
C     GIVEN AN INITIAL VALUE OF ROO, RO IS CALCULATED USING THE NEWTON
C     RAPHSON TECHNIQUE FOR SOLVING IMPLICIT EQUATIONS IN ONE UNKNOWN.
   15 FX=-FUNC+((ROO+1.)/ROO)*DLOG((1.-ROO*B)/(1.-ROO*A))
      FFX=-(1./(ROO*ROO))*DLOG((1.-ROO*B)/(1.-ROO*A))-((ROO+1.)/ROO)*((B
     6-A)/((1.-ROO*B)*(1.-ROO*A)))
      RC=ROO-FX/FFX
      WRITE(6,150)RO
C     RO IS THE INITIAL VALUE OF R
      IF(RO-1./B)17,17,18
   18 L=L+1
      GO TO 19
   17 DELTA=(10.**(-7.))
      IF(DABS(RO-ROO)-DELTA)10,10,14
   14 ROO=RO
      GO TO 15
   10 WRITE(6,350)AMPS,XO,RO
      C=FLOAT(N)
      DR=-RO/C
      WRITE(6,200)PL,PR,PPOS,A,B
      WRITE(6,250)TK,EW,ETH,SCLRT,SIGI
      WRITE(6,400)
      DO 700 I=1,N
      D=FLOAT(I-1)
C     INCREMENT THE PARAMETER R AS FOLLOWS:
      R=RO+D*DR
C     FOR ANY VALUE OF R, THE TIME, THICKNESS AND VOLTAGE ARE
C     CALCULATED.
```

```
      E=ETH-(RG*TK/F)*DLOG((1.-R*B)/(1.-R*A))
C     E IS THE CELL VOLTAGE.
      CONST=AREA*AREA*RG*TK*SIGI*FF/(VOL*F*AMPS*AMPS*3600.)
      T=(CONST/2.)*((2.+2./R+1./(R*R))*DLOG((1.-R*B)/(1.-R*A))-(2.+2./RO
     3+1./(RO*RO))*DLOG((1.-RO*B)/(1.-RO*A))+(2.*B+B*B)*DLOG(((1.-R*B)*R
     40)/((1.-RO*B)*R))-(2.*A+A*A)*DLOG(((1.-R*A)*RO)/((1.-RO*A)*R))+(B-
     5A)*(1./R-1./RO))
C     T IS THE TIME IN HR.
      IF(T-200.)13,13,300
   13 X=(AREA*SIGI*(10.**8.)/AMPS)*((R+1.)/R)*(ETH-E)
C     X IS THE SCALE THICKNESS IN ANGSTROMS.
      XOC=DSQRT(XO*XC+2.*RATE*T*(10.**16.))
C     XOC IS THE THICKNESS ONE WOULD CALCULATE AT OPEN CIRCUIT OR R=-1.
      WRITE(6,500)R,T,E,X,XOC
  700 CONTINUE
  300 CONTINUE
    4 FORMAT(I3)
  180 FORMAT('0',12X,'RO')
  150 FORMAT(5X,D15.8)
  100 FORMAT(2(4X,D11.4),7X,I3)
  200 FORMAT('0',4X,'PL=',D11.4,4X,'PR=',D11.4,4X,'PPOS=',D11.4,4X,'A=',
     7D11.4,4X,'B=',D11.4)
  250 FORMAT('0',4X,'TK=',D11.4,4X,'EW=',D11.4,4X,'ETH=',D11.4,4X,'SCLRT
     8=',D11.4,4X,'SIGI=',D11.4)
  350 FORMAT('0',4X,'AMPS=',D11.4,4X,'XC=',D11.4,4X,'RO=',D15.8)
  400 FORMAT('0',12X,'R',17X,'TIME',17X,'E',14X,'THICKNESS',15X,'XOC')
  500 FORMAT(5(5X,D15.8))
      STOP
      END
$ENTRY
$STOP
```

APPENDIX F. FORTRAN COMPUTER PROGRAM FOR CALCULATING THE GALVANOSTATIC SCALING KINETICS OF SILICON IN OXYGEN GAS ASSUMING THE CONSTANT t_{ion} MODEL

```
//D201JH19  JOB  'U3191,TIME=3,SIZE=128K',HINZE
//STEP1  EXEC  WATFIV,REGION.GO=128K
//GO.SYSIN  DD  *
$JOB            U3191HINZE,TIME=10,PAGES=40
C      THIS PROGRAM CALCULATES THE GALVANCSTATIC SCALING KINETICS OF
C      SILICON IN OXYGEN GAS.  THE CONSTANT IONIC TRANSFERENCE NUMBER
C      MODEL IS ASSUMED FOR THE CALCULATION.
       REAL*8 FF,F,ETH,RG,TK,DSQRT,Y,SCLRI,VOL,B,AMPS,XO,EW,SCLRT,TION,A,
      1SIGT,EO,C,DX,DABS,DLOG,D,X,Z,T,XOC,AREA,TEL,E
       FF=96500.
       F=23062.
       ETH=1.754
       AREA=1.
       RG=1.987
       TK=1123.
       VOL=6.825
C      FF AND F ARE THE FARADAY NUMBER IN COUL/EQ AND CAL/VOLT CM,
C      RESPECTIVELY, ETH IS THE THERMODYNAMIC EMF, RG IS THE GAS CONSTANT
C      TK IS THE TEMPERATURE IN DEGREES KELVIN, VOL IS THE EQUIVALENT
C      VOLUME.
       SCLRT=5.088*(10.**(-16.))
C      SCLRT IS THE SCALING RATE CONSTANT IN EQ/CM SEC.
       B=VOL*SCLRT*3600.*(10.**16.)
C      B IS THE SCALING RATE CONSTANT IN SQUARE ANGSTROMS/HR.
       READ(5,5)L
       DO 900 K=1,L
       READ(5,90)Y
C      Y IS THE RATIO OF THE IONIC SCALING RATE CONSTANT TO THE TOTAL
C      SCALING RATE CONSTANT.
       SCLRI=Y*SCLRT
C      SCLRI IS THE IONIC PART OF THE SCALING RATE CONSTANT.
       READ(5,4)M
       DO 700 J=1,M
       READ(5,100)AMPS,XO,EW,N
C      AMPS IS THE TOTAL CURRENT, XO IS THE INITIAL THICKNESS IN
C      ANGSTROMS AND EW IS THE OPEN CIRCUIT EMF.
       TION=EW/ETH
```

```
      TEL=1.-TION
C     TION AND TEL ARE, RESPECTIVELY, THE IONIC AND ELECTRONIC
C     TRANSFERENCE NUMBERS.
      A=(VOL*TION*AMPS*3600.*(10.**8.))/(FF*AREA)
C     A IS THE ELECTROLYSIS RATE IN ANGSTROMS/HR.
      SIGT=(2.*SCLRI*F*FF)/(3.*RG*TK*TION*TEL)
C     SIGT IS THE TOTAL CONDUCTIVITY AT PO2=1 ATM.
      EC=EW-(2.*F*XO*ETH*AMPS*(10.**(-8.)))/(3.*AREA*RG*TK*SIGT)
C     EO IS THE INITIAL CELL VOLTAGE.
      WRITE(6,200)ETH,EW,SCLRT,TION,B
      WRITE(6,250)A,SIGT,EO,Y
      WRITE(6,350)AMPS,XO,SCLRI
      C=FLOAT(N)
      DX=(DABS(B/A)-XO)/C
      WRITE(6,400)
      DO 300 I=1,N
      D=FLOAT(I-1)
C     INCREMENT THE THICKNESS AS FOLLOWS:
      X=XO+(D*DX)
C     X IS THE THICKNESS IN ANGSTROMS.
      E=EW-(2.*F*X*ETH*AMPS*(10.**(-8.)))/(3.*AREA*RG*TK*SIGT)
C     E IS THE CELL VOLTAGE.
      Z=(B+A*XO)/(B+A*X)
      T=(X-XO+(B/A)*DLOG(Z))/A
C     T IS THE TIME IN HOURS.
      XOC=DSQRT(XO*XO+2.*B*T)
C     XOC IS THE THICKNESS ONE WOULD EXPECT AT OPEN CIRCUIT.
      WRITE(6,500)T,X,E,XOC
  300 CONTINUE
  700 CONTINUE
  900 CONTINUE
    5 FORMAT(I3)
   90 FORMAT(4X,D11.4)
    4 FORMAT(I3)
  100 FORMAT(3(4X,D11.4),7X,I3)
  200 FORMAT('0',4X,'ETH=',D11.4,4X,'EW=',D11.4,4X,'SCLRT=',D11.4,4X,'TI
     2ON=',D11.4,4X,'B=',D11.4)
```

```
  250 FORMAT('0',4X,'A=',D11.4,4X,'SIGT=',D11.4,4X,'EO=',D11.4,4X,'Y=',D
     311.4)
  350 FORMAT('0',4X,'AMPS=',D11.4,4X,'XO=',D11.4,4X,'SCLRI=',D11.4)
  400 FORMAT(12X,'T',19X,'X',19X,'E',18X,'XOC')
  500 FORMAT(4(5X,D15.8))
      STOP
      END
$ENTRY
$STOP
```

APPENDIX G. FORTRAN COMPUTER PROGRAM FOR CALCULATING THE GALVANOSTATIC SCALING KINETICS OF SILICON IN OXYGEN GAS ASSUMING THE CONSTANT σ_{ion} MODEL

```
//D201JH18  JOB  'U3191,TIME=3,SIZE=128K',HINZE
//STEP1  EXEC  WATFIV,REGION.GO=128K
//GO.SYSIN  DD  *
$JOB            U3191HINZE,TIME=07,PAGES=40
C      THIS PROGRAM CALCULATES THE GALVANOSTATIC SCALING KINETICS OF
C      SILICON IN OXYGEN GAS. THE CONSTANT IONIC CONDUCTIVITY MODEL IS
C      ASSUMED FOR THE CALCULATION.  NEUTRAL TRANSPORT IS NEGLECTED.
       REAL*8 PR,PL,PPOS,EW,ETH,F,FF,DEXP,RG,TK,BETA,SIGI,A,B,DLOG,E,R,RO
      1,VOL,AREA,X,T,AMPS,CONST,ALPHA,SCLRT,C,DR,D,FUNC,DEL,Z,DABS,XOC,RA
      2TE,DSQRT,ROO,FX,FFX,DELTA,XO
       RG=1.987
       FF=96500.
       F=23062.
       TK=1123.
       VOL=6.825
       AREA=1.
       PL=10.**(-31.5)
       PR=1.
       ETH=(RG*TK/(4.*F))*DLOG(PR/PL)
C      RG IS THE GAS CONSTANT, FF AND F ARE, RESPECTIVELY, THE FARADAY
C      NUMBER IN COUL/EQ AND CAL/VOLT EQ, TK IS THE ABSOLUTE TEMPERATURE,
C      VOL IS THE EQUIVALENT VOLUME, PL IS THE OXYGEN  PRESSURE AT THE
C      SI,SIO2 INTERFACE, PR IS THE OXYGEN  PRESSURE AT THE SIO2,O2
C      INTERFACE, ETH IS THE THERMODYNAMIC EMF.
       READ(5,5)L
       DO 900 K=1,L
       READ(5,170)EW
C      EW IS THE OPEN CIRCUIT EMF.
       ALPHA=DEXP((ETH-EW)*F/(RG*TK))
       PPOS=((PR**0.25-ALPHA*PL**0.25)/(ALPHA-1.))**4.
C      PPOS IS THE OXYGEN PRESSURE AT WHICH THE IONIC AND HOLE
C      CONDUCTIVITIES ARE EQUAL.
       A=(PL/PPOS)**0.25
       B=(PR/PPOS)**0.25
       RATE=1.25*10.**(-11.)
C      RATE IS THE SCALING RATE CONSTANT IN SQUARE CM/HR.
       SCLRT=RATE/(VOL*3600.)
```

```
C      SCLRT IS THE SCALING RATE CONSTANT IN EQ/CM SEC.
       BETA=DLOG((1.+B)/(1.+A))
       SIGI=SCLRT*F*FF/(RG*TK*BETA)
C      SIGI IS THE IONIC CONDUCTIVITY.
       READ(5,4)M
       DO 300 J=1,M
       READ(5,100)AMPS,XO,N
C      AMPS IS THE TOTAL CURRENT AND XO IS THE INITIAL THICKNESS IN
C      ANGSTROMS.
       WRITE(6,180)
       FUNC=AMPS*XO*F*(10.**(-8.))/(AREA*SIGI*RG*TK)
       ROO=0.99/B
C      GIVEN AN INITIAL VALUE OF ROO, RO IS CALCULATED USING THE NEWTON
C      RAPHSON TECHNIQUE FOR SOLVING IMPLICIT EQUATIONS IN ONE UNKNOWN.
   15  FX=-FUNC+((ROO+1.)/ROO)*DLOG((1.-ROO*B)/(1.-ROO*A))
       FFX=-(1./(ROO*ROO))*DLOG((1.-ROO*B)/(1.-ROO*A))-((ROO+1.)/ROO)*((B
     6-A)/((1.-ROO*B)*(1.-ROO*A)))
       RO=ROO-FX/FFX
       WRITE(6,150)RO
C      RO IS THE INITIAL VALUE OF R
       DELTA=(10.**(-7.))*(10.**(-4.*RO))*(10.**(-2.3*DLOG(B)))
       IF(DABS(RO-ROO)-DELTA)10,10,14
   14  ROO=RO
       GO TO 15
   10  WRITE(6,350)AMPS,XO,RO
       C=FLOAT(N)
       DR=-RO/C
       WRITE(6,200)PL,PR,PPOS,A,B
       WRITE(6,250)TK,EW,ETH,SCLRT,SIGI
       WRITE(6,400)
       DO 700 I=1,N
       D=FLOAT(I-1)
C      INCREMENT THE PARAMETER R AS FOLLOWS:
       R=RO+D*DR
C      FOR ANY VALUE OF R, THE TIME, THICKNESS AND VOLTAGE ARE
C      CALCULATED.
       E=ETH-(RG*TK/F)*DLOG((1.-R*B)/(1.-R*A))
```

```
C       E IS THE CELL VOLTAGE.
        CONST=AREA*AREA*RG*TK*SIGI*FF/(VOL*F*AMPS*AMPS*3600.)
        T=(CONST/2.)*((2.+2./R+1./(R*R))*DLOG((1.-R*B)/(1.-R*A))-(2.+2./RO
       3+1./(RO*RO))*DLOG((1.-RO*B)/(1.-RO*A))+(2.*B+B*B)*DLOG(((1.-R*B)*R
       40)/((1.-RO*B)*R))-(2.*A+A*A)*DLOG(((1.-R*A)*RO)/((1.-RO*A)*R))+(B-
       5A)*(1./R-1./RO))
C       T IS THE TIME IN HR.
        X=(AREA*SIGI*(10.**8.)/AMPS)*((R+1.)/R)*(ETH-E)
C       X IS THE SCALE THICKNESS IN ANGSTROMS.
        XOC=DSQRT(XO*XO+2.*RATE*T*(10.**16.))
C       XOC IS THE THICKNESS ONE WOULD CALCULATE AT OPEN CIRCUIT OR R=-1.
        WRITE(6,500)R,T,E,X,XOC
  700 CONTINUE
  300 CONTINUE
  900 CONTINUE
    5 FORMAT(I3)
  170 FORMAT(4X,D11.4)
    4 FORMAT(I3)
  180 FORMAT('0',12X,'RO')
  150 FORMAT(5X,D15.8)
  100 FORMAT(2(4X,D11.4),7X,I3)
  200 FORMAT('0',4X,'PL=',D11.4,4X,'PR=',D11.4,4X,'PPOS=',D11.4,4X,'A=',
      7D11.4,4X,'B=',D11.4)
  250 FORMAT('0',4X,'TK=',D11.4,4X,'EW=',D11.4,4X,'ETH=',D11.4,4X,'SCLRT
      8=',D11.4,4X,'SIGI=',D11.4)
  350 FORMAT('0',4X,'AMPS=',D11.4,4X,'XO=',D11.4,4X,'RO=',D15.8)
  400 FORMAT('0',12X,'R',17X,'TIME',17X,'E',14X,'THICKNESS',15X,'XOC')
  500 FORMAT(5(5X,D15.8))
        STOP
        END
$ENTRY
$STOP
```

ACKNOWLEDGMENTS

The author wishes to thank his major professor, Dr. John W. Patterson, for his encouragement and guidance through the course of this investigation. The author is indebted to John Baker of Dow Corning Corporation for providing the silicon specimens and to Frederick Schmidt of the Ames Laboratory, Jon Schieltz of Tektronix, Incorporated and to Joseph Singer of NASA Lewis Research Center for providing the platinum electrodes used in this study. Thanks are also due to the Aerospace Research Laboratories for sponsoring this research. Last, but certainly not least, the author wishes to express gratitude to his wife, Ann, for her love, support and patient understanding through all the years of his graduate study.